J. Fluid Mech. (1979), *vol.* 94, *part* 4, *pp.* 673–709
Printed in Great Britain

Conditional sampling study of the turbulent wake of a cylinder. Part 1

By GRACIO FABRIS
Illinois Institute of Technology, Chicago†

(Received 16 January 1978 and in revised form 6 December 1978)

The far turbulent wake of a slightly heated cylinder was studied using our specially developed four-wire probe and digital processing of signals obtained. The processing method included a simultaneous solution of full nonlinear response equations for the four sensors yielding values of instantaneous velocity vector and temperature. The accuracy of results was improved substantially by the subtraction of free-stream velocity and temperature variations, first-order corrections for the d.c. drift of the signals, the elimination of 60 Hz related noise, and instantaneous correction for the streamwise displacement between the sensor wires. A low temperature threshold was used to discriminate between turbulent and potential flow.

The frequency of crossing of the turbulent–potential interface and statistics of turbulent and potential zone intervals are presented. Conditionally sampled fluctuating velocity and temperature fields are given for turbulent and potential zones as well as for a fluid at the downstream and upstream interface of the turbulent zones. Averaging was done with respect to conventional (Reynolds) as well as local zone or point means. The results on turbulence structure up to second-order correlations are presented in this paper.

It is hoped that the data will be useful for those interested in methods of prediction of turbulence, especially those based on the consideration of large structures. Researchers more interested in the physical phenomena involved might also find the data suitable for further analysis and interpretation.

1. Introduction

The jet, the wake and the mixing region flows are free turbulent shear flows. The mixing region has been studied by Liepmann & Laufer (1947) and more recently, with conditional sampling, by Wygnanski & Fiedler (1970) and by Spencer (1970). The early insight into free turbulent jets, both two-dimensional and axisymmetric, was provided by Corrsin (1943) and Corrsin & Uberoi (1949, 1950). Some of the modern comprehensive studies of plane jets were conducted by Bradbury (1965), Goldschmidt & Young (1973), Jenkins (1975) and Kotsovinos (1975), while Wygnanski & Fiedler (1969) studied in depth the turbulent axisymmetric jet.

The first hot-wire investigations of the near wake of a circular cylinder were carried out by Kovasznay (1948) and by Roshko (1954). The far wake was studied and described in depth in four papers by Townsend three decades ago (1947, 1948, 1949*a*, *b*).

† Present address: Argonne National Laboratory, Argonne, Illinois, 60439.

0022–1120/79/4289–7400 $02.00

In this pioneering effort he measured the mean and fluctuating magnitudes of all three velocity components and the Reynolds stresses, as well as the transport of heat and of turbulent kinetic energy at a number of downstream stations. Ten years later Grant (1958) measured all nine correlation coefficients at one station, 533 diameters downstream of the cylinder, and speculated on the large-scale structure of the turbulence. In the last decade Alexopoulos & Keffer (1968) repeated some of Townsend's measurements. Their measurements showed differences in values and shape of the profile of the normal velocity fluctuations v' from Townsend's results (1947). Keffer also considered the behaviour of wakes under straining (1965, 1967). Freymuth & Uberoi (1969) measured spectra in an axisymmetric wake and then extended their work to the turbulent temperature field and to correlations which involve temperature (1971).

The conditional sampling technique has made it possible to extract much more information from flow experiments. Also the recent availability of analog to digital conversion and the processing of signals in large digital computers greatly increased the scope of experimental techniques. The improvement of experimental probes and techniques further enhanced the capability of flow experiments.

A number of conditional sampling studies have been performed in the last few years. However, for various reasons only a minority of these have been on the wake flow. The two recent studies of two-dimensional wakes using conditional sampling were not published until after our investigation was well under way. However, they dealt with a much smaller set of variables than in the present study. Thomas (1973) concentrated on the streamwise velocity component and on the statistics of the turbulent–non-turbulent interface. Working in the same facility as Townsend, but with modern instrumentation, Thomas provided corroborative evidence for Townsend's measurements but also found some discrepancies with the generation-old data. LaRue (1974) used conditional sampling and digital computing techniques similar to ours in the investigation of the nature of temperature fluctuations in a warm cylinder wake for a Reynolds number of 2800 at downstream stations of 400 and 500 diameters. His treatment of frequency response, detection of the interface based on temperature, and errors associated with finite sampling times are of special significance to the present study.

In the present investigation, our conditional sampling of temperature and all three components of velocity by a single four-wire probe, combined with digital processing of the data, provides considerably more simultaneous field information than the studies of Thomas and LaRue. Part of the present study then complements the Thomas and LaRue single-wake investigations, with less emphasis on the interface statistics and more stress on the technologically important transport processes supplied by double and triple correlations. (These data are to be presented in part 2.) The unplanned overlap with the work of LaRue was fortunate since comparison with his sophisticated results was favourable and provides confidence in the reliability of our techniques.

2. Experimental apparatus

2.1. *The wind tunnel*

The experiments were made in the IIT environmental wind tunnel. The test section is 3 ft high, 2 ft wide and 12 ft long. This section is preceded by a 4:1 contraction, ten fine-mesh screens and a honeycomb made of packed 8 in. long plastic soda straws, 0·125 in. diameter.

A traversing mechanism was used to move the probe in the x (streamwise) direction and in the y (lateral) direction perpendicular to the wake-generating horizontal cylinders. Marks on both plexiglass sidewalls were references for lateral and streamwise positions of the probe.

Downstream of the test section a $\frac{1}{2}$ in. gap in the wind tunnel means that the static pressure in the tunnel is equal to the pressure in the room and also mechanically isolates the test section from the diffuser and motor. Fine-mesh screen placed at the end of the test section raised the pressure in it to 0·01 in. of water above atmospheric pressure, ensuring that no leaks into the test section could separate the wall boundary layers.

Often the probe had to be inserted 2 feet or more into the test section. The original probe made of a $\frac{5}{16}$ in. tube vibrated at the tip. The main cause of these vibrations was the tunnel oscillations induced by a blower; these were eliminated by mechanically decoupling the test section from the rest of the tunnel. Occasional probe vibrations due to vortex shedding from its stem was remedied by the use of streamlined tubing for the probe support.

2.2. *Conditions in the test section*

Profiles of u' and v' were measured to check the background flow conditions in the test section. Two-point space–time correlations were used for diagnostic discrimination between vorticity and pressure-associated velocity fluctuations. Four kinds of fluctuations were found originally to exist in the test section.

First, slow quasi-periodic fluctuations with periods of 3–10 s and peak-to-peak excursions of $0{\cdot}015U_\infty$ (r.m.s. $0{\cdot}005U_\infty$) were observed. These fluctuations might be caused by the effective Helmholtz oscillator between the room and the tunnel volumes. Since these volumes communicate through multiple unequal openings little could be done further to verify the speculation or to eliminate the condition.

Most low-speed wind tunnels have similar fluctuations though they are rarely recognized and reported. Thomas (1973) and LaRue (1974) mentioned such fluctuations. These fluctuations are usually unnoticed because the threshold of most r.m.s. meters is around 1 Hz. Some investigators observe such fluctuations on their memory oscilloscopes but ignore them as having irrelevantly large scales with respect to the flow phenomena under scrutiny. However, in experiments like ours long averaging times may be required even for measurements of $\overline{U}$. In our case, the analog averaging time of 10 s reduced the peak-to-peak U amplitudes only about sevenfold from the cited 'non-averaged' level of $0{\cdot}015U_\infty$. This cannot be considered satisfactory when we are measuring a small velocity defect in the far wake.

Secondly, higher-frequency fluctuations (5–10 Hz) were observed to occur almost simultaneously in the whole test section with a peak-to-peak U amplitude of the order of 1 per cent of the free-stream speed (r.m.s. $0{\cdot}0035U_\infty$). These fluctuations are pressure rather than vorticity associated: as longitudinal waves they consist primarily of u disturbances. Indeed, the original (pre-compensation) measurements indicated highly anisotropic disturbances dominated by u fluctuations. It is believed that these variations of pressure were caused by the air-conditioning system of the experimental room. Ultimately, we were able to mitigate the major effects of these two types of relatively slow variations by a scheme of compensation (to be discussed later).

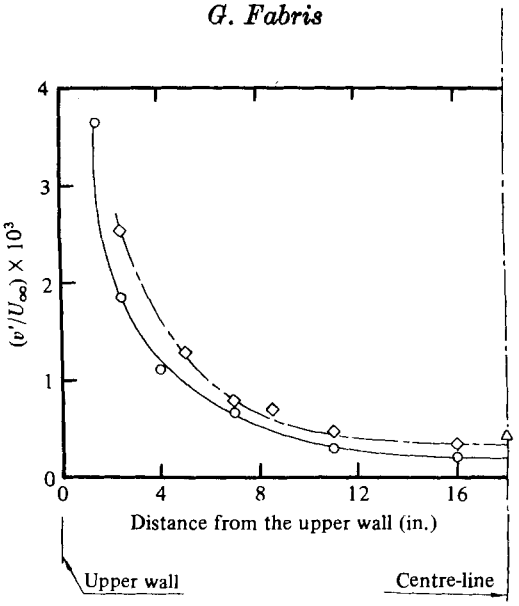

FIGURE 1. Lateral fluctuation intensities in the empty tunnel. $U_\infty = 6{\cdot}46$ m s^{-1}; ——○——, $x/D = 60$; ——– – ——◇——, $x/D = 300$; △, $x/D = 400$.

The third type of fluctuation was related to vorticity-associated eddies which were passing through the screens and were convected at free-stream speeds. The amplitude of these fluctuations was comparable to those of the first two kinds. These fluctuations were essentially eliminated by installing the plastic drinking straws honeycomb (length to cell diameter ratio of 64) just upstream of the screens.

The fourth type of fluctuation was potential fluctuations induced by the $\frac{1}{2}$ in. thick turbulent boundary layers on the test section walls. These fluctuations propagated downstream at speeds slower than that of the free stream. Their amplitude is an order of magnitude smaller than those of the first two types, and we need to keep in mind their possible influence only as the walls of the tunnel are approached (see figure 1).

When the first two types of fluctuations (consisting mostly of u') are instantaneously subtracted from the signals as it was possible to do in our experiments, the remaining free-stream fluctuations at the centre-line of the tunnel at $x/D = 400$ registered the levels of $u'/U = 0{\cdot}00055$, $v'/U = 0{\cdot}00042$ and $w'/U = 0{\cdot}0007$. Figure 1 displays the variation of the lateral fluctuations across the upper half of the empty test section. This component of the free-stream fluctuations which is perpendicular to the cylinder is more likely to influence the wake formation, in particular its 'flapping'. The measured v' level is comfortably low and we have seen no evidence of any flapping behaviour. It should be mentioned that to measure such low levels of fluctuations special care must be taken to decrease the noise of all the equipment. Our calibration and correction procedures are described by Fabris (1978).

The static pressure change along the test section at a velocity of 6·46 m s^{-1} is given in figure 2. The pressure drop coefficient along the 2·54 m of the test section where the wake was studied is $C_p = \Delta P/\frac{1}{2}\rho U^2 = 0{\cdot}0362$. Pressure gradients of such small magnitude are not expected to influence the dynamics of the turbulence in the wakes.

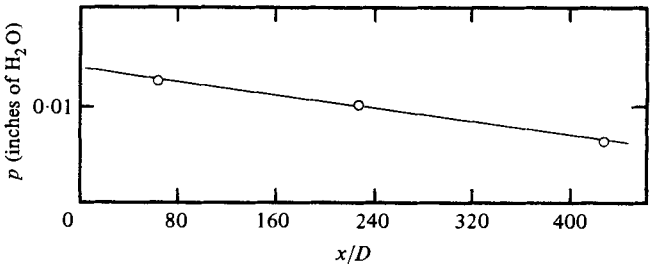

FIGURE 2. Change of static pressure along the test section.

It took usually about six hours of continuous tunnel running to reach a steady temperature in the test section. However, even then the temperature would occasionally vary up to 0·05 °C during a 15 min period. Such temperature drifts were compensated for by subtracting signals of the temperature probe-wire from a reference temperature wire.

It is difficult to judge the free-stream temperature fluctuations after the above drift signals are eliminated, since the noise level in the temperature signals is higher than that in the velocity signals. Θ' measured from the reference-subtracted signals in the free stream was 0·0014 °C which is considerably less than Θ' inferred from a single uncompensated measurement.

2.3. *Diagnostic of the wake flow*

Considerable exploration of the wake flow was undertaken before the final conditions of our experiments were fixed. A Calrod cylinder with a nominal diameter of 6·25 mm and length of 0·762 m was placed on the centre-line of the tunnel at the upstream end of the test section and supported by the walls of the test section.

Figure 3 shows the $\overline{U}$ and u' spanwise profiles at the centre-plane of the wake of the cylinder. The results indicate that two-dimensionality of the flow is satisfactory over three-fourths of the wake span. To minimize the interaction of the cylinder with the sidewall boundary layers several other ways of supporting the cylinder were attempted. None of them, however, decreased the sidewall effects seen in figure 3.

Diagnostic tests were performed to select a satisfactory heating level of the cylinder. One of the more informative experiments is summarized in figure 4. Displacement of the wake due to cylinder heating would be most positively detected by placing a horizontal wire at the two symmetric wake positions with maximum slope, $|\partial u'/\partial y|_{\max}$, and watching the fluctuating voltage output as the heater is turned on and off. An upward wake shift due to buoyancy, integrated over the length of 2·54 m, would be reflected in a positive difference $e_{\text{upper}} - e'_{\text{lower}}$, as is the case for maximum heating of the cylinder in figure 4. For $\overline{\Theta}/\overline{\Theta}_{\max}$ centre-line values less than 0·5, no measurable buoyancy effects appear to be present.

In order to minimize possible heating effects on the boundary-layer separation from the cylinder and on the early instability of the separated shear-layer, conditions corresponding to the centre-line $\overline{\Theta}/\overline{\Theta}_{\max}$ value of 0·25 were chosen. With our fine temperature sensor the wake overheat of 0·34 °C at $x/D = 400$ was ample for satisfactory detailed measurements. Results presented later confirm the above choice:

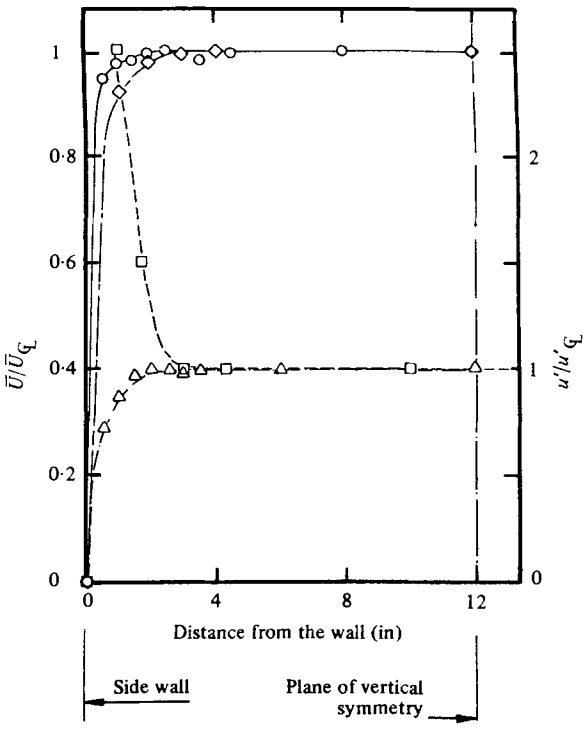

FIGURE 3. Spanwise velocity measurements at wake centre-line. $U_\infty = 6{\cdot}46$ m s^{-1}. $x/D = 3$: —○—, $\bar{U}/\bar{U}_{\mathfrak{C}}$; — · —△— · —, $u'/u'_{\mathfrak{C}}$. $x/D = 230$: — · —◇—, $\bar{U}/\bar{U}_{\mathfrak{C}}$; — —□— —, $u'/u'_{\mathfrak{C}}$.

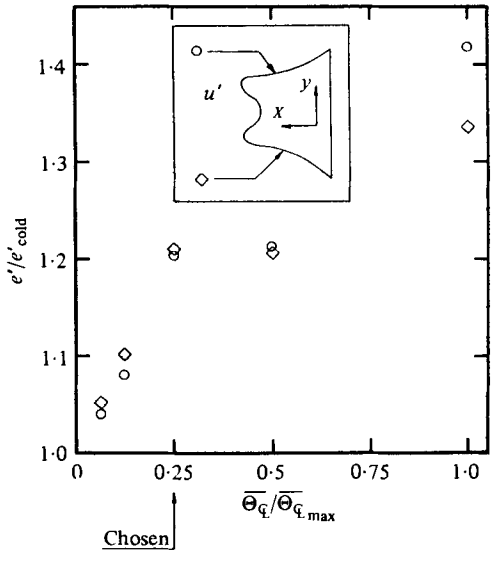

FIGURE 4. Voltage fluctuation changes at the upper and lower sensitive positions as a function of cylinder heating; $U_\infty = 6{\cdot}46$ m s^{-1}; $\Theta_{\max} = 1{\cdot}35$ °C; $x/D = 400$; ○, upper wake side; ◇, lower wake side.

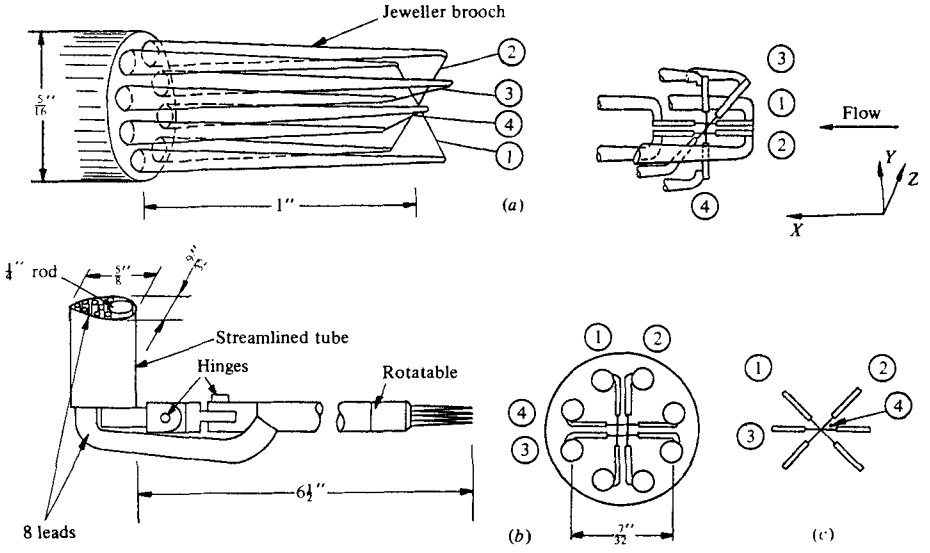

FIGURE 5. The four-wire probe. (*a*) Top view; (*b*) front view; (*c*) side view of sensors only, $d = 0{\cdot}625\ \mu$m.

within the accuracy of our measurements the mean and fluctuating velocity fields are unaffected by this mild heating.

We note in figure 4 that the voltage fluctuations increase even for mild heating when u' levels should remain unaffected. This rise reflects the temperature sensitivity of the constant-temperature anemometer. In fact, in a later analysis we have introduced a correction to velocity measurements owing to temperature effects. Since $u(t)$ and $\theta(t)$ are not perfectly correlated the rise in e' would not be expected to be linear but the peculiar break in the data is somewhat puzzling. However, since it does not vitiate the diagnostic conclusions of negligible buoyancy effect there is no need for speculation or concern.

2.4. *The four-wire probe and experimental equipment*

A special four-wire probe (figure 5) was designed and made by the author for this study. A number of advances were made in the data-processing method. The probe and the processing method are the subject of another paper (Fabris 1978).

Four platinum/10 % rhodium wires of $0{\cdot}625\ \mu$m diameter were used. The length of the supporting prongs was increased, their diameter decreased, their mutual distance increased three times, relative to commercial single-wire probes, thus making the probe practically interference-free. The processing method included several corrections: those for a streamwise displacement of sensors based on instantaneous convection velocity, for d.c. drifts in all channels during data acquisition, for instantaneous variation of free-stream tunnel velocity and temperature as well as for the computation of all 60 Hz-related noise and its subtraction from all channels. Full, nonlinear response equations for all four sensors were written, reflecting influence of all three components of velocity and temperature. These equations were solved simultaneously using the rapidly converging Newton–Raphson numerical technique

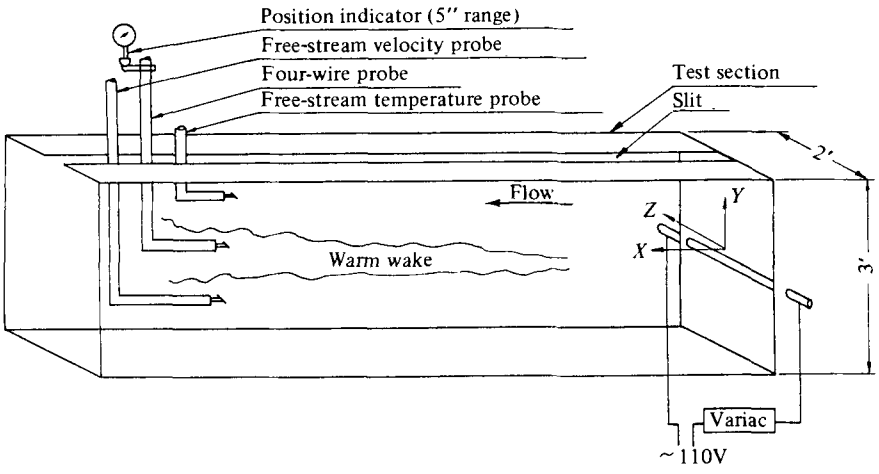

FIGURE 6. Experimental arrangement in the test section.

yielding in principle correct instantaneous values of the three components of velocity and temperature at a point.

To assure that the system (probes, calibrations, processing, and correction technique) was functioning properly as a whole, it was checked extensively using established analog methods. For example, several u', v', and w' wake profiles were measured, each profile by using three different analog methods or probes. Also, the cold wake was rotated 90° within the tunnel by mounting the cylinder vertically while the four-wire probe remained fixed and results were compared.

Improvement in accuracy achieved by applying this processing method was indicated by the low 'turbulence intensity' measured in the free stream and by the low r.m.s. of temperature fluctuations, and also by measurements of steady values of very small but existent mean lateral velocity in the far wake.

Figure 6 is a schematic representation of the disposition of the three probes and the wake in the test section. The wake was generated by a Calrod cylinder located at the centre-line of the tunnel. The wake was sampled with the four-wire probe while the free-stream velocity and temperature were simultaneously monitored with two single-wire probes.

Standard DISA constant-temperature anemometry units, linearizers, and filters were used. Predominantly temperature-sensing wires were operated at very low overheat in constant-current mode. To minimize noise the constant-current bridge was home built using a Philbrick Nexus operation manifold board. Extended testing of different temperature-measuring set-ups resulted in the final improvement in signal-to-noise ratio about thirty times over that of commercial constant-current anemometry equipment.

For the acquisition and digitizing of data the minicomputer PDP 11/10 was used with auxiliary equipment including an analog-to-digital converter.

3. Processing of data

The data acquisition program digitized the four signals from the four-wire probe simultaneously. The free-stream velocity signal of a much lower frequency content was digitized with a time delay of 0·115 ms with respect to the first four signals. The sampling frequency was chosen to be twice the highest frequency of interest in the flow, in accordance with the Nyquist sampling theorem. Thus the chosen sampling frequency was 400 Hz while low-pass filters were set at 2000 Hz to avoid aliasing.

Because of the limitations in the capacity of the minicomputer memory the digitized signals were transferred to the magnetic tape in records of finite time lengths with time gaps between the records. The records contained 1440 sequences of five digital values for the five channels. The time lapse between sequences was 0·25 ms so that one record covered 0·358 s of data. The 0·358 s duration of records of continuous data was long enough for all the computations reported here as well as for computations of correlation functions and power spectra.

The data acquisition program was written in such a way that all records were triggered on line (i.e. each record starts at the same phase of the 60 Hz cycle). This enabled us to subtract the repetitive part of the signals and obtain signals 'cleaned' of practically all the 60 Hz-related noise which formed a major part of the noise in all channels.

3.1. *Choice of lateral sampling positions: procedures in experimental runs*

The number of lateral sampling positions was a compromise between the desire for finer information and budget limitations. We decided on twelve lateral positions covering the upper side of the wake, the centre-line and one position below the centre-line. The analog measurements had indicated that the wake was symmetrical, and there was no necessity to take measurements in the lower side of the wake. The spacing between lateral positions was 7·366 mm at $x/D = 400$ and 0·604 mm at $x/D = 200$.

During the data acquisition runs the probe was first placed in the free stream as far from the tunnel centre-line as the traversing mechanism allowed. Signals were sampled at this position for about 15 s, with 6 s of actual data being stored. Then the probe was moved in steps to cover twelve positions in the wake. The probe was each time moved back to the original free-stream position and the signals sampled again to provide information on repeatability and d.c. drifts in the signals during the recording of each profile. The time at the start of data acquisition for each position was recorded (see Fabris 1978).

3.2. *Generation of the intermittency function*

The intermittency function $I(t)$ is defined as zero in potential flow and unity in turbulent, i.e. vortical, flow. For fluids with a molecular Prandtl number near unity, the vorticity and temperature interfaces between potential and turbulent regions coincide within the accuracy of any measurements. For our purposes we defined $I(t)$ to be unity inside the heated wake flow and zero in the uncontaminated 'cold' flow outside the wake.

To help the decision on the level of a discrimination threshold a number of detailed plots of temperature signal in intermittent flow were made. They revealed that fluctuations in the unheated flow (mostly noise) were of short duration: one or two

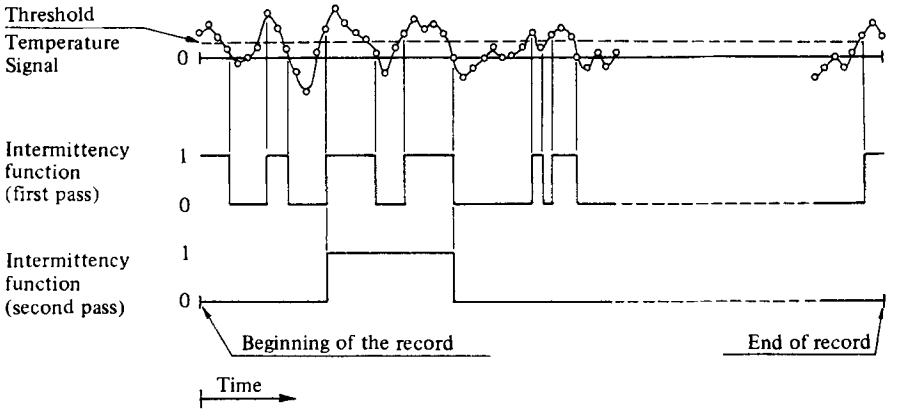

FIGURE 7. Generation of the intermittency function.

digital time steps (hereafter called instants). However, even the shortest and the least overheated signals were of lower frequency and longer duration. This justified the introduction of 'hold time' similar to that used by LaRue (1974) and Kovasznay & Kibens (1968) to bridge over short time periods when the signal crosses the threshold level and returns back immediately so that this excursion is attributed to signal noise rather than to an extra short genuine warm spot or cold spot. LaRue (1974) presents an exhaustive analysis of the factors influencing the choice of the threshold and hold time.

We chose the threshold to be 0·017 °C and 0·013 °C at x/D of 200 and 400 respectively. This choice corresponds to approximately 4 per cent of the mean maximum temperature overheat in the wake. The hold time was chosen to be 0·75 ms, which corresponds to three digital time steps or instants.

We varied the threshold level and the hold time to find effects on the intermittency factor and the bursting frequency as suggested by LaRue (1974). However, effects were minimal. The reason for this is that the noise level in our temperature signal was very low, making the discrimination threshold about ten times higher than r.m.s. of the noise level, but yet quite low with respect to actual temperature fluctuations in heated fluid.

Figure 7 gives more direct insight into the decision processes and generation of the intermittency function on the basis of threshold and hold-time criteria. For illustrative purposes, Figure 7 presents only the border-line cases while the typical temperature signals in the heated flow reached much higher levels and experienced longer durations.

3.3. *Computed flow quantities*

One of the objectives of this investigation was to document the behaviour of the terms involving velocity and temperature fields in the basic turbulence equations for the incompressible wake flow. Another objective was to provide more statistical and physical insight into the turbulence structure in the wake. We therefore computed the various types of averages and moments characterizing the different flow aspects.

Eleven different averages were calculated for most computed quantities. These comprised conventional averages and conditional averages: (a) in turbulent (heated)

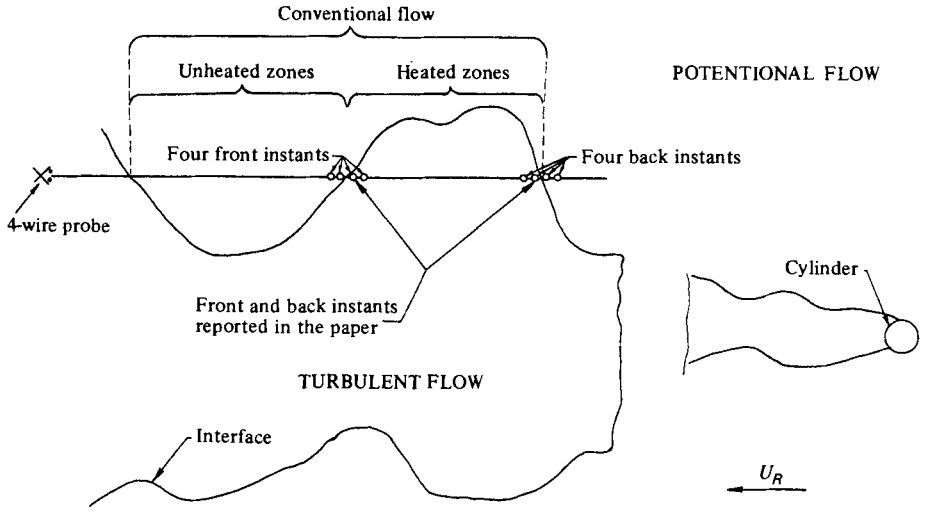

FIGURE 8. Scheme for instants of conditional sampling.

zones; (*b*) in cold zones; (*c*) in four ensembles consisting of the four ordered instants around the front of turbulent zones; and (*d*) in four ensembles consisting of the four ordered instants around the back of turbulent zones. These definitions are illustrated in figure 8 which gives the schematic representation of the instants or positions ordered with respect to the interface for which the separate ensemble averages were computed.

Nine different averages were calculated for all quantities involving time derivatives not presented in this paper. They comprised the groups (*a*) to (*d*) above except that in groups (*c*) and (*d*) the three conditional ensemble averages involved three rather than four instants around the interface.

Most of the averaged quantities were referred to three different levels as base, see figure 9. The so-called Reynolds or R-averages used in the conventional means over the full elapsed time as zero levels of fluctuations. The zone or Z-averages utilized the conditional mean over the heated or cold zones as zero level of fluctuations in that zone. Finally, averages were also referred to the free-stream properties as base.

3.4. *Stationarity of the averaged flow quantities*

The question arises as to the total length of signals needed to yield values of the averaged flow quantities within acceptable errors of their true ensemble averages. Figure 10 illustrates the change in the averages over elapsed time t of four statistical variables in one realization at the centre-line of the wake at $x/D = 400$. The total time of data presented on figure 10 was six seconds. The question is whether the final value of the averages, denoted by the subscript f, is sufficiently close to the value obtained if t increased indefinitely.

Lumley & Panofsky (1964) gave several criteria for choosing the averaging time interval and achieving a desired level of accuracy. These criteria were used by Hedley & Keffer (1974) and led to rather long required time intervals primarily because they were based on fractional departures from the local y-dependent values of the ensemble averages of the variables. To seek small fractional departures uniformly across the

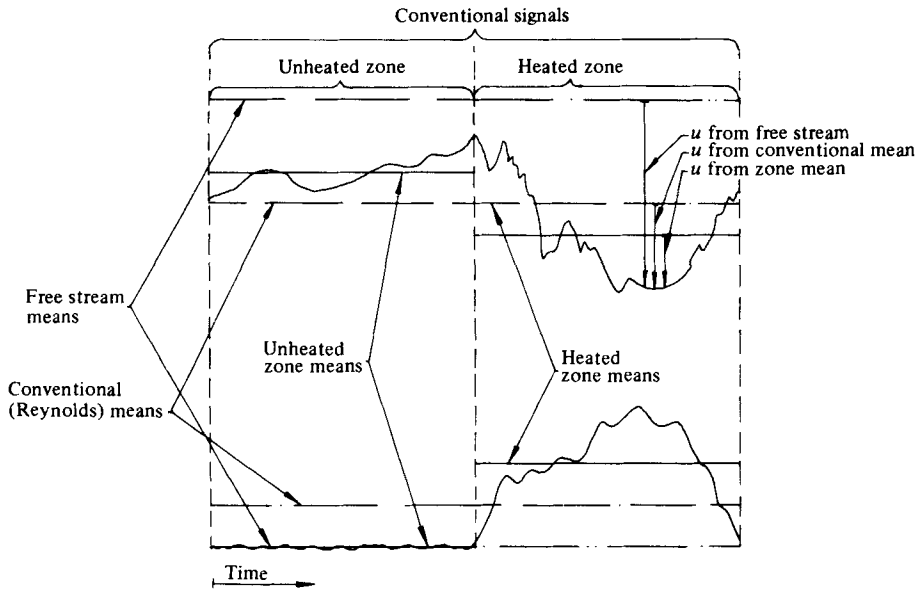

FIGURE 9. Scheme of averaging with respect to different bases.

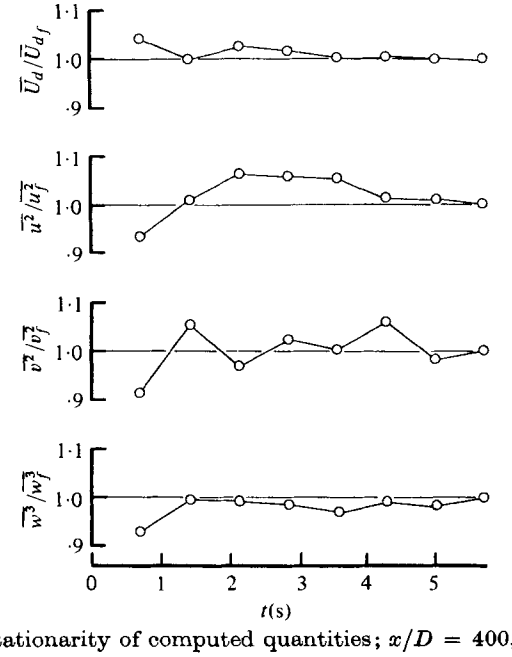

FIGURE 10. Stationarity of computed quantities; $x/D = 400$, wake centre-line.

profiles placed unnecessarily stringent requirements on the averaging time. One would prefer to give more weight to accuracy obtained through the 'main body of the profiles' rather than in the shallow tails at the intermittent edges of the wake.

We fell back on the formulas for 95 per cent confidence intervals in Gaussian processes (see Crow, Davies & Maxfield 1960). Turbulence at the centre-line behaves in many respects in approximately Gaussian pattern. However, to ensure that flow

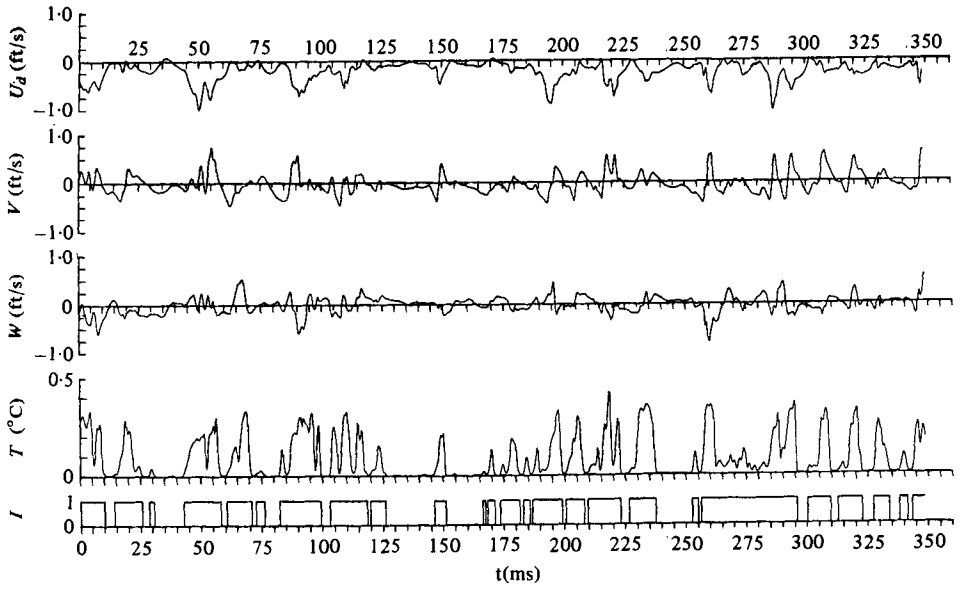

FIGURE 11. Instantaneous flow quantities at $x/D = 400$, $y/D = 7{\cdot}2$, $\gamma = 0{\cdot}65$.

variation at two different times corresponds to completely 'independent events', one could separate them by at least two integral time lengths. We used Grant's measurements in a cylinder wake (1956) and spaced events so far apart that no correlation existed between them. In this way we established that 6 s measurements covered approximately 200 completely independent events. (Or 400 events if each integral scale is considered as an independent event.)

Using the 95 per cent confidence interval formula, we then estimated that 6 s data would give average velocities and temperatures within 3 per cent of the maximum 95 per cent of the time; within 1·5 per cent of the maximum 70 per cent of the time; and within one per cent of the maximum 50 per cent of the time. The accuracy in the r.m.s. values of most fluctuating quantities in the study was estimated to be approximately 30 per cent lower than the preceding estimates. While one always wishes for better accuracy, the real criterion of a compromise is whether the main objectives have been met. Comparisons of our results with those of others suggest that the choice of 6 s for the total time interval was justified. The degree of consistency of the information for the wake should speak for itself.

We believe that our subtraction of the free-stream velocity and temperature variations has practically eliminated slow drafts in the output. This has contributed to the achievement of steady values within shorter time intervals.

4. Instantaneous quantities

Let us first focus on the instantaneous picture at a point to provide a 'feel' for the nature of the flow under scrutiny, keeping in mind that no finite number of correlations can describe it fully. Figure 11 displays traces of instantaneous flow quantities obtained by digital processing at $x/D = 400$ and $y/D = 7{\cdot}2$, corresponding to an

intermittency factor of $\gamma = 0{\cdot}65$. While the turbulent field is clearly random in character, some quasi-repeatable patterns are discernible. An exhaustive discussion on the question of the presence and importance of the nonrandom processes is given by Roshko (1976). The fact that the coherent structures exhibit a wide distribution of size and mutual distances and are obliterated by truly random turbulent process has been responsible for the rather late recognition of their existence by Papailiou (1971), Bevilaqua & Lykoudis (1971) and by Brown & Roshko (1971).

Let us single out an isolated short turbulent bulge at time $t = 150$ ms on figure 11. It has a lower streamwise velocity than the potential patches upstream and downstream of it. There is a virtual coincidence of the heated (turbulent) region and the region of rapidly changing lateral velocity. The front (downstream) part of this turbulent entity is moving rather rapidly toward the wake centre-line (negative V) while its back part is moving in the opposite direction. The minimum of the streamwise velocity seems to occur approximately at the time of the maximum positive time derivative of the lateral velocity but with some shift to a region of the outward-moving fluid. The trace of the spanwise velocity indicates increased movement in the spanwise direction compared to the upstream and downstream potential flow patches. The temperature increases on the downstream side of the turbulent bulge in 'ramp'-like manner (see Antonia, Prabhu & Stephenson 1975), while the decrease on the upstream side is rather abrupt.

A more or less similar flow pattern is repeated a number of times. Differences in sizes, mutual time shifts and obliteration by smaller eddies are present as explained by Roshko (1976). Generally, decreases of the streamwise velocity are somewhat more rapid than its increases. Changes to the outward motion are more rapid than changes to the inward motion. Time derivatives of the lateral velocity seem to reach the highest values. One could say that the sharpest gradients in lateral velocity correspond to 'rolling over' of turbulent bulges by a faster-moving potential flow that produces strong spanwise vorticity. Quite frequently sharp gradients are present in the spanwise velocity suggesting a possibility that some of the strong vortices could turn from a spanwise to a lateral direction. In the literature (Roshko 1976) there is talk of a possible 'vortex loop formed by pinching off and joining together of vortices from opposite sides of the street' (wake).

5. Distributions of intermittent turbulent and potential fluid

With the increasing number of conditional sampling studies and serious attempts to take into account large structures in turbulent shear flows, the statistics of the distributions of the turbulent flow interface have become more important. Good discussions are given by Hedley & Keffer (1974) of the turbulent boundary layer and LaRue & Libby (1976) of the two-dimensional wake flow.

Figure 12 displays profiles of the intermittency factor plotted in self-similar coordinates ($l_0 = [(x - x_0)\,D]^{\frac{1}{2}}$, $x_0 = -40D$) on Gaussian distribution probability paper. Good agreement with Gaussian distribution can be seen. The small difference between the two downstream positions may be due to the fact that the two-dimensional wake is not yet self-preserving at a downstream location of $x/D = 200$.

Figure 13 displays the bursting frequency distribution normalized by the free-stream velocity and the self-similar length scale. Bursting rate is defined here as the

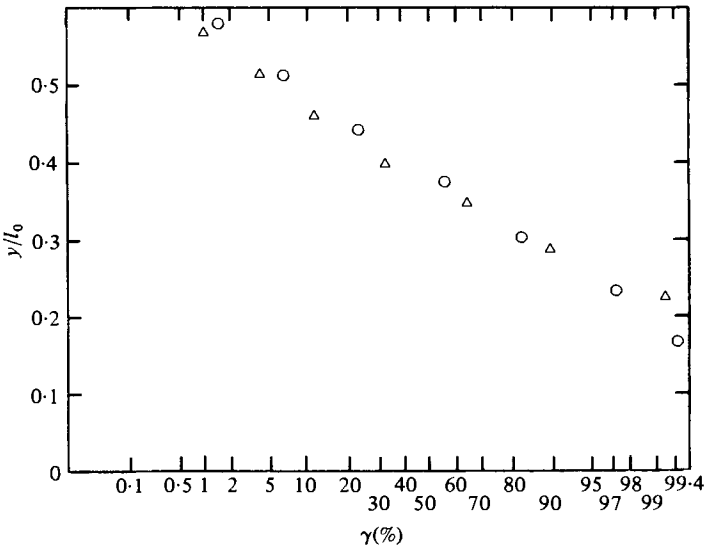

FIGURE 12. Distribution of intermittency factor. ○, $x/D = 200$; △, $x/D = 400$.

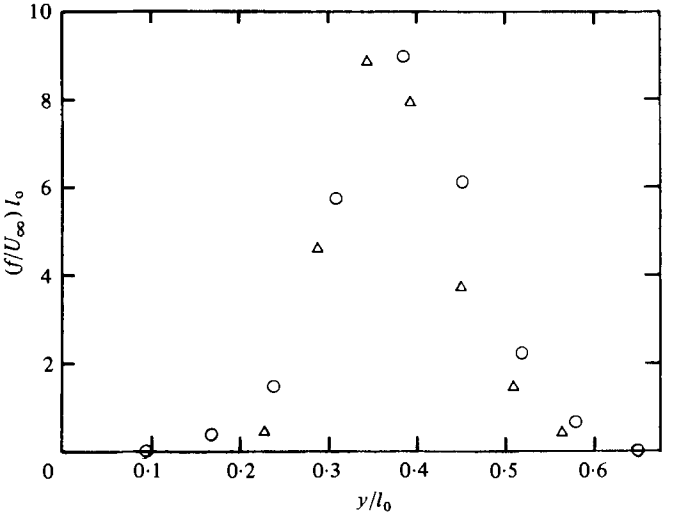

FIGURE 13. Distribution of bursting frequency. ○, $x/D = 200$; △, $x/D = 400$.

rate of crossings of the fronts of turbulent bulges at the particular position. Reasonable agreement at two locations is obtained. However f_γ is more sensitive than γ to the establishment of self-similarity, and some differences at two locations are present.

A number of bursting-frequencies graphs are presented for different turbulent shear flows. However, the bursting frequencies were not measured at two distinctly different locations to find out possible differences. At the first downstream location the intermittent region seems to be wider in self-similar co-ordinates; this is especially true of regions of low f_γ. We can only speculate that this might be a side effect of stronger vortices at that location.

Statistical properties of turbulent and potential fluid time intervals will be given in this section. 'Complete cycle' intervals were also studied by noting the time interval

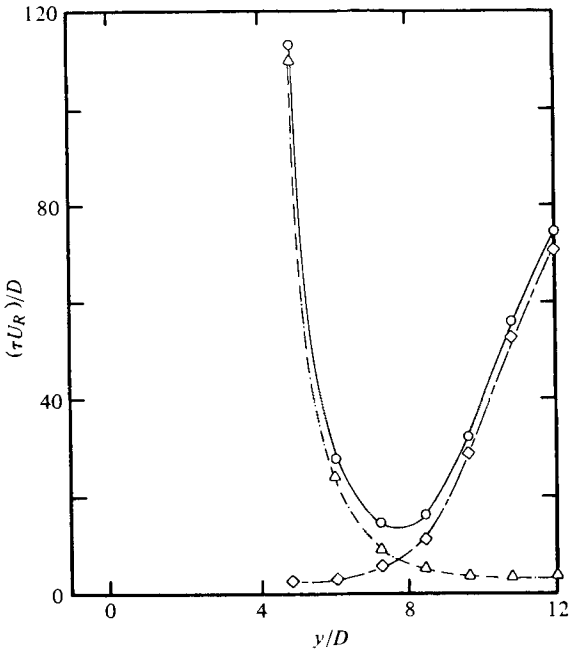

FIGURE 14. Time lengths of intermittency intervals, $x/D = 400$. ———○———, back–back; ———◇———, back–front; — · —△— · —, front–back.

between the back of one turbulent bulge and the back of the next turbulent bulge. Thomas (1973) studied in addition front–front time intervals but found that they did not differ appreciably from back–back intervals.

The data reduction program could not account for time intervals shorter than 0·75 ms or longer than 350 ms. Figure 14 gives average time lengths of intermittency intervals normalized by the ratio D/U_R. Close to the wake centre potential cold flow intervals are short but they increase in length dramatically toward the wake periphery. The opposite situation exists with the turbulent flow intervals.

Average time lengths between the backs of two adjacent turbulent bulges are equal to the sum of the two previous lengths. This curve is really a reciprocal of the f_γ profile. Deviation from symmetry can be more easily noticed in this plot.

Figure 15 displays the standard deviation of time-length intervals, indicating the variation in the lengths of intermittent intervals. Trends are similar to average time-length trends.

Figure 16 compares standard deviation to mean length of the intermittent intervals. In these non-dimensional co-ordinates full cycle back-to-back intervals deviate the least from their mean value in the centre of the intermittent region. At positions where mean lengths of potential or turbulent intervals become shorter, deviations from these means become smaller even in these less emphasizing non-dimensional co-ordinates.

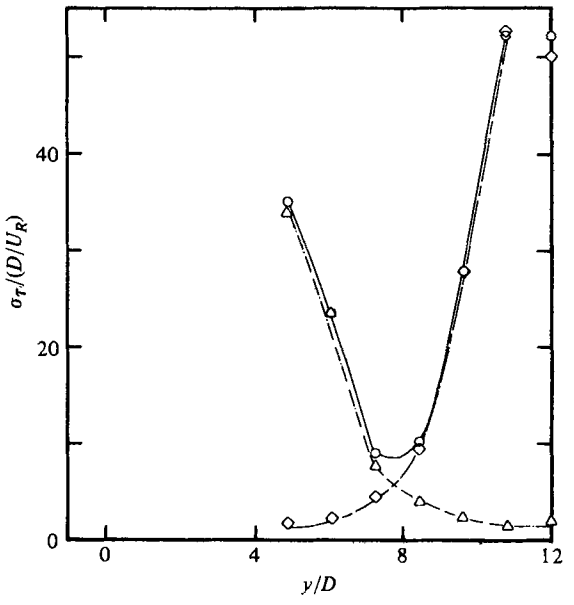

FIGURE 15. Standard deviation of intermittency intervals, $x/D = 400$; symbols the same as for figure 14.

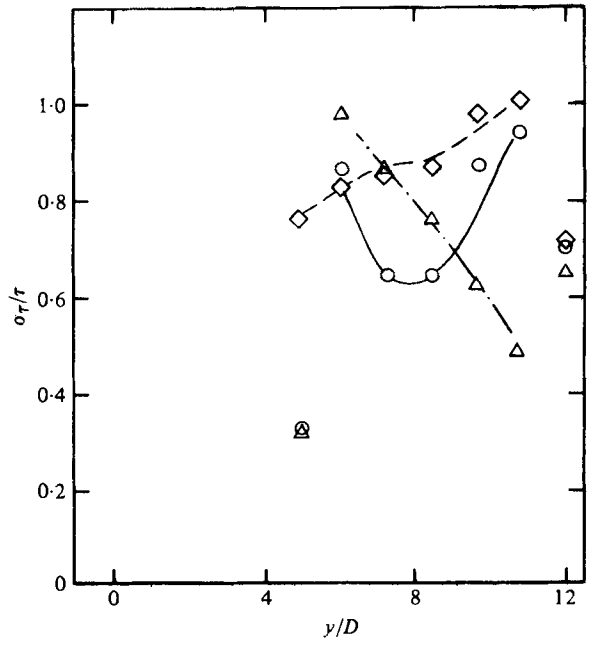

FIGURE 16. Ratio of standard deviation to mean lengths for intermittency intervals, $x/D = 400$; symbols the same as for figure 14.

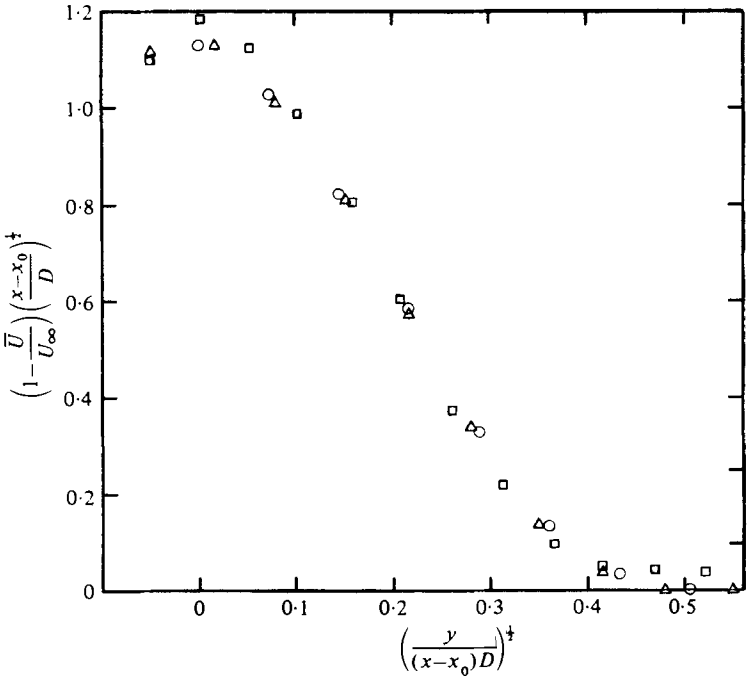

FIGURE 17. Distribution of mean streamwise velocity defect in similarity co-ordinates; △, $x/D = 200$; □, $x/D = 400$; ○, $x/D = 160$ (Thomas 1973).

6. Mean flow quantities

6.1. *Streamwise velocity*

Figure 17 displays the velocity defects at two locations plotted together with Thomas (1973) data in self-similar co-ordinates. These data have already been used by Libby (1976) in his prediction model of the intermittent turbulent wake.

The far-wake conservation of the velocity defect (e.g. Hinze 1959, p. 385) seems to be approximately satisfied. In the framework of such a linearized approximation the defect velocities exhibited here could be superposable only if displacement effects were taken into account. The emphasis here being on the fluctuating field, however, intermediate mean profiles were not studied in a systematic manner.

Figure 18 exhibits the conditional streamwise velocity defects. Zone averages in unheated (potential) and heated (turbulent) flow regions as well as point averages at the front and back of heated bulges (first and last instants within turbulent flow) are also indicated. The patches of potential flow are collectively moving faster than the average flow at all lateral positions. This difference increases as the potential flow penetrates closer to the wake centre-line. However, these inner potential patches are moving slower than the free stream: in other words, they have been decelerated by interaction with even slower turbulent bulges. This deceleration can be accomplished only through pressure since the potential flow has not experienced any internal shear stresses or 'mixing'.

The turbulent bulges in turn move slower than the average flow, as should be expected. The maximum difference is not as high as that for the potential flow; this is probably a consequence of the profile shape of the convential mean velocity defect.

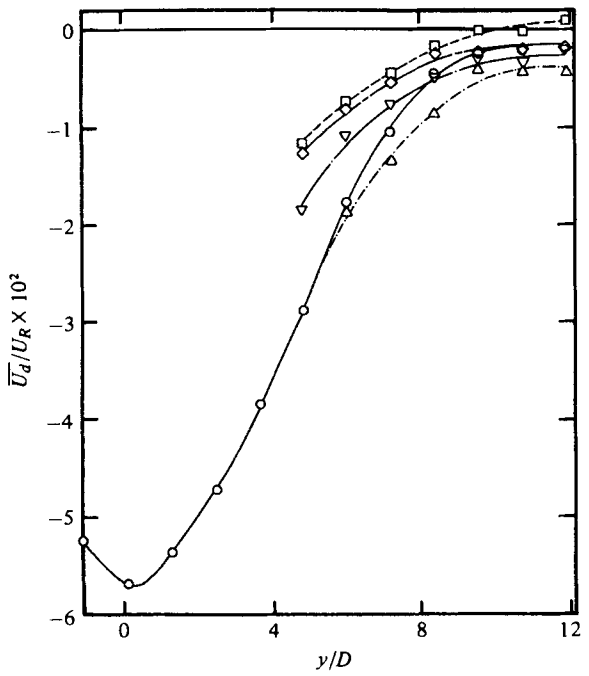

FIGURE 18. Conditional streamwise velocities, $x/D = 400$. R-averaged: ——○——, conventional; —◇— - —, potential zones; — · —△— · —, turbulent zones; — —□— —, turbulent fronts; —▽— · —, turbulent backs. Full symbols, Z-averaged (used in later figures).

On the average, the fluid at the back is slower moving than the potential average but faster than the average turbulent flow. This is interesting, as some might expect the the opposite: namely, that the potential flow would be more likely to 'push' the backs of turbulent bulges than to 'suck' the front. This may have some relationship to the known fact that a sink works more efficiently than a source jet flow. Positive differences between the velocities at the fronts and backs of turbulent bulges are consistent with the observed lengthening of the turbulent bulges. The propagation of the turbulent interface via entrainment diffusion of the vorticity is superposed on it.

6.2. *Lateral velocity*

Figure 19 displays the conditional mean lateral velocities at $x/D = 400$. The conventionally averaged velocity has a small negative value showing that there is a net inflow toward the wake centre-plane. In many relevant papers, measurements of this lateral velocity are not reported since experimental points are usually very scattered. The fact that our experimental trends are consistent should provide confidence in the steadiness and the reliability of our results. The potential flow moves towards the wake centre-line and the average velocity of potential lumps which penetrate farther inward increases with closeness to the wake centre-line. The turbulent flow moves away from the wake centre-line, increasing the average velocity with lateral distance: the lesser number of turbulent lumps which are propelled with farthest outward momentum.† The lateral

† Note that in addition to the fluid velocity the turbulent potential interface propagates into the potential fluid by diffusion of the vorticity. The propagation velocity can be measured only by two-point correlations.

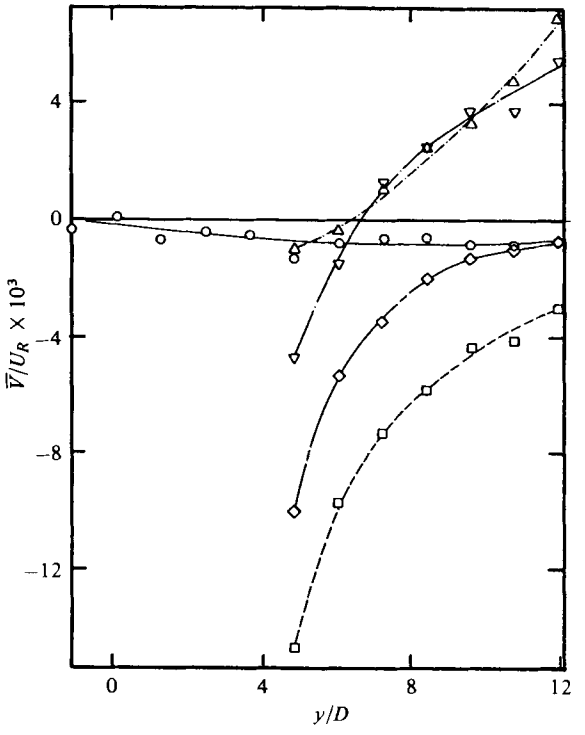

FIGURE 19. Conditional lateral velocities, $x/D = 400$. Symbols the same as for figure 18.

velocity of the warm turbulent fronts can be viewed approximately as the lateral velocity of the cold backs. Accordingly the interpretation of the motion of the warm fronts as being very nearly that of the *avant-garde* of cold potential lumps is plausibly consistent with the more negative mean velocity of these points in figure 19. In fact, for $y/D = 8$ or so, where the probable length of the cold potential lumps is smaller, their average lateral velocity represents a plausible mean of the lateral velocities of the fronts and backs of the warm regions.

The spanwise vorticity component is $\omega_z = \partial V/\partial x - \partial U/\partial y$. Calculating its mean values for potential and turbulent zones indicated that potential zones indeed have no vorticity while the turbulent zones have.

These results together with those of figure 18 are essentially consistent with those found by Blackwelder & Kovasznay (1972) and Hedley & Keffer (1974) in the outer regions of the turbulent boundary layers. It is as if turbulent bulges were 'rolled' in the direction of mean velocity.

6.3. *Temperature distributions*

Temperature distributions were extensively investigated for a similar geometry by LaRue (1974) at downstream locations at $x/D = 400$ and 500. The locations being relatively close to each other and probably in a self-preserving region no difference was noticed in conditional levels of temperature in the turbulent bulges at two locations. We conducted measurements at $x/D = 200$ and 400. Figure 20 compares these temperatures plotted in self-similar co-ordinates. Conventional averages show only a slight discrepancy at two locations. The conditional temperatures in the outer part

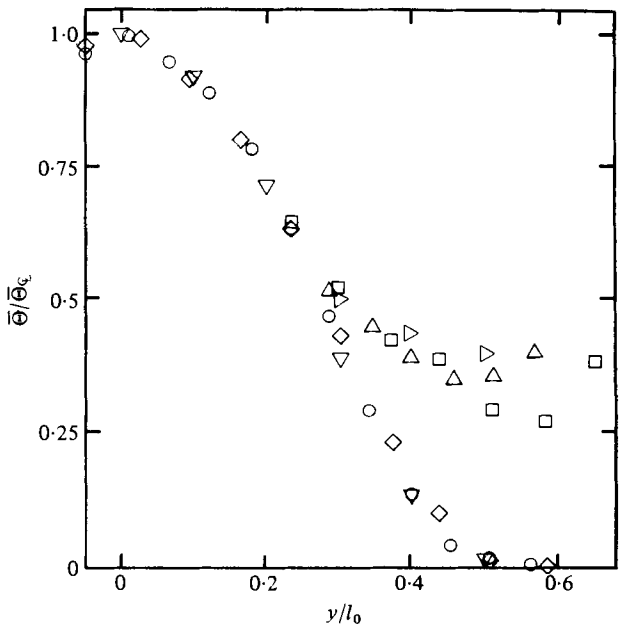

FIGURE 20. Conditional mean temperatures, $x/D = 400$: ○, conventional; △, turbulent zones. $x/D = 200$: ◇, conventional; □, turbulent zones. LaRue (1974), $x/D = 400$: ▽, conventional; ▷, turbulent zones.

of the turbulent bulges show somewhat more measurable differences. At the first downstream location, turbulent bulges move somewhat further outwards (in self-similar co-ordinates) and their average temperature is lower. A possible cause of this could be a relatively increased entrainment to outer parts of the bulges due to higher lateral and streamwise velocity differences between potential and turbulent bulges at $x/D = 200$ (see Fabris 1974). LaRue's (1974) data at $x/D = 400$ is also given showing good agreement with our data.

We also recorded average temperatures at 'front' and 'back' (downstream and upstream edges) of the turbulent bulges. These temperatures are of course just above the discrimination threshold temperature (equal to 0·013 °C at $x/D = 400$). However, data (see figure 22 in Fabris (1974)) show that temperature slopes $\overline{\partial\Theta/\partial t}$ are higher at the upstream edge of turbulent bulges. The average slope increases more and more as one moves further outwards from the wake centre-line, indicating a thinner interface as discussed by LaRue & Libby (1974).

7. Mean squared fluctuating quantities

In this section we will present profiles of mean squares of fluctuating quantities u^2, v^2, w^2, θ^2 and q^2. As we discussed earlier, there are at least three ways of computing such fluctuations. Only those with more physical significance will be described here.

7.1. *The streamwise fluctuation component*

Figure 21 presents the streamwise component of fluctuations. Open symbols are R-averages and full symbols are Z-averages. The conventional average has the familiar maximum approximately at the position of maximum $\partial\overline{U}/\partial y$ (see figure 18). There the

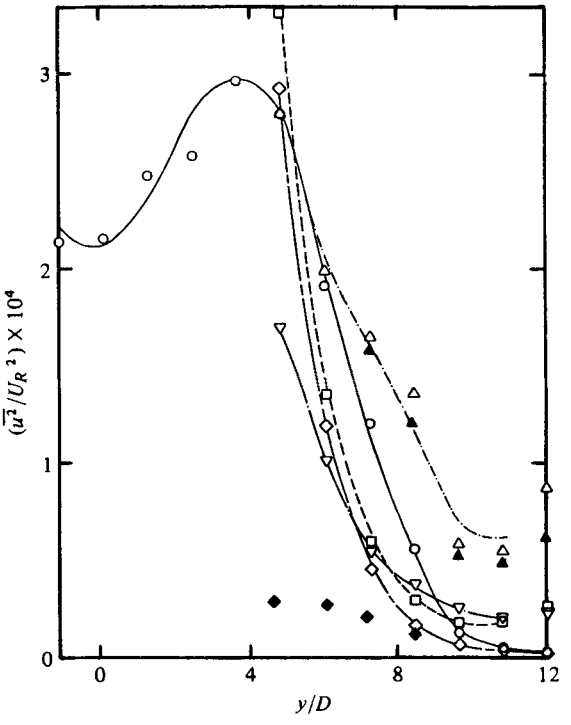

FIGURE 21. Streamwise fluctuations, $x/D = 400$. Symbols the same as on figure 18.

production of turbulence is highest. It will be seen from figure 28 that the other contributing factor, $-uv$, also peaks in this vicinity. The value at the centre-plane is high even though the shear stress $-uv$ as well as the gradient $\partial\overline{U}/\partial y$ and hence the dominant production of turbulence there vanish. The conventional average naturally decreases to zero past the edge of the wake. The turbulent zone average however does not drop to zero at the wake edge.

The fluctuations of the potential fluid with respect to the local mean velocity increase with closeness to the wake centre and apparently may even exceed the conventionally computed averages. The level of the fluctuations at the turbulent fronts always exceeds that in the potential flow, by an almost constant magnitude. The fluctuations of the turbulent backs at the wake edge are higher than those in the potential flow, while close to the wake centre the order is reversed.

Z-averages give the levels of the fluctuations in the turbulent and potential zones with respect to their own zone mean velocities (obtainable from figure 18). The values of fluctuations at the fronts and backs have less direct physical meaning when computed in this way; however, they do represent standard deviations of the corresponding probability density curves.

The zone-referenced fluctuations in the turbulent zones are only slightly weaker than the corresponding 'Reynolds' fluctuations. The fluctuations within the potential flow and at the fronts and backs of the turbulent regions do increase with proximity of the central region of the wake, but the values are much lower than the R-averages. The Z-averages of the backs of the heated lumps appear decidedly higher than those of the fronts. This could indicate more agitation at the backs (see also figure 25).

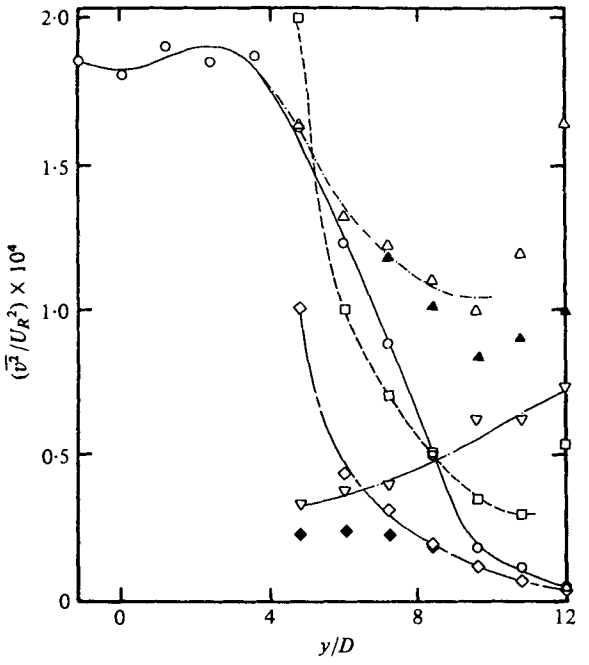

FIGURE 22. Conditional lateral fluctuations; $z/D = 400$; symbols the same as on figure 18.

7.2. *The lateral fluctuation component*

Figure 22 shows that the conventional average of v^2 has two separate peaks with a very small valley at the wake centre-plane. This shape with a shallow valley between two small peaks has been reported recently by Alexopoulos & Keffer (1968) but Townsend (1947, 1949*a*) found only a single maximum located at the centre-plane having about two times higher values than $\overline{u^2}$ and $\overline{w^2}$. We were aware of this possible discrepancy in Townsend's data early in our research and have searched all available literature on two-dimensional wake and jet flows. The same reason led us to perform extra-careful and repeated calibrations and diagnostic checks. Based on these considerations we believe that our data are correct.

Conditional curves on figure 22 behave basically like those of the longitudinal turbulent component in figure 21, except for the behaviour of the backs of the turbulent lumps. However, the fluctuations in the turbulent lumps retain relatively higher levels at the edge of the wake. Similarly, the zone-averaged data resemble those for $\overline{u^2}$. Again, the zone averages indicate larger local agitation at the backs as compared to the fronts of the heated zones.

7.3. *The spanwise fluctuation component*

Figure 23 presents the fluctuations in the spanwise direction. In contrast to the $\overline{u^2}$ and $\overline{v^2}$ cases the difference between the standard and the Z-averages is negligible and we have not shown the later data. It is due to the fact that all computed conditional W averages are practically zero.

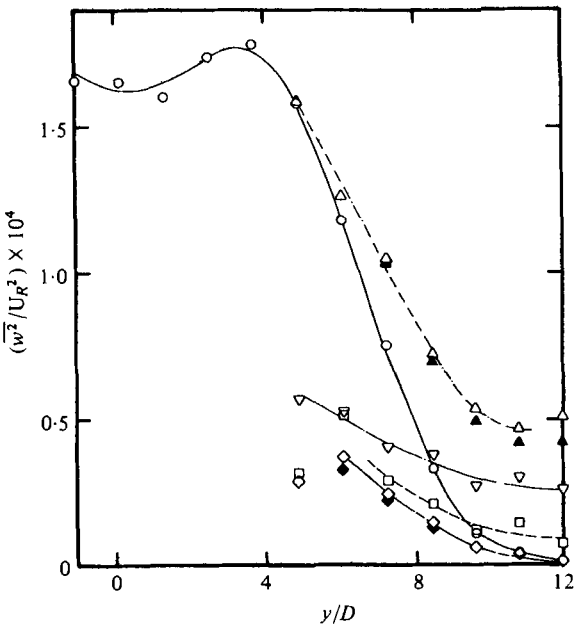

FIGURE 23. Conditional spanwise fluctuations, $x/D = 400$; symbols the same as on figure 18.

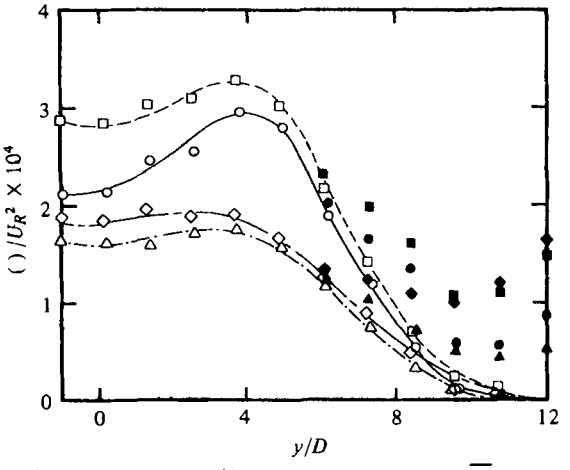

FIGURE 24. Turbulent energy, $x/D = 400$. ——○—— $\overline{u^2}$; ——— — —◇——, $\overline{v^2}$; — · —△— · —, $\overline{w^2}$; — — —□— —, $\frac{1}{2}\overline{q^2}$; full symbols are R-averages in turbulent regions.

7.4. *Kinetic energy of fluctuations*

Figure 24 shows a comparison of the three components of the conventionally averaged fluctuations as well as the turbulent kinetic energy

$$\tfrac{1}{2}\overline{q^2} = \tfrac{1}{2}(\overline{u^2}+\overline{v^2}+\overline{w^2}).$$

The streamwise component has the highest peak, an observation consistent with the view that it absorbs energy directly from the mean flow and primarily in the vicinity of the inflexion points of the mean velocity profile. The lateral and spanwise components are about 35 per cent lower, but approach the $\overline{u^2}$ level at the wake centre-plane. At the wake edge the lateral fluctuations are higher than fluctuations in the other two

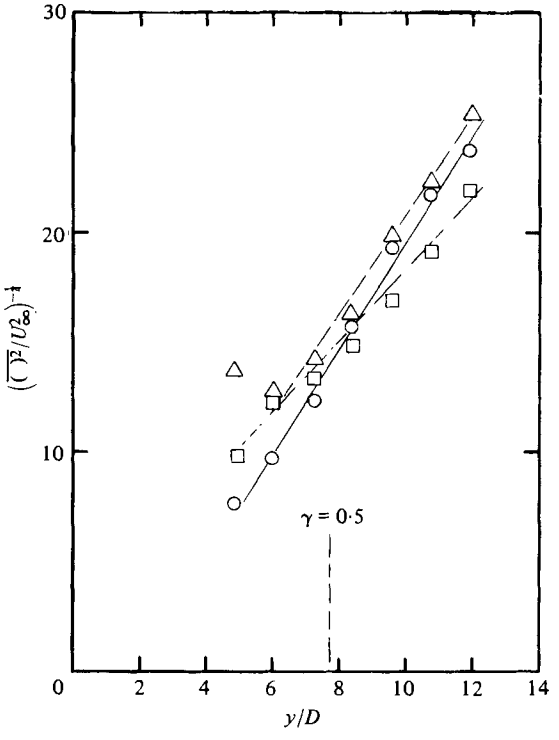

FIGURE 25. Decay of intensity of fluctuations in intermittent potential regions, R-averaged, $x/D = 400$. —○—, $(\overline{u^2}/U_\infty^2)^{-\frac{1}{4}}$; — · —□— · —, $(\overline{v^2}/U_\infty^2)^{-\frac{1}{4}}$; — —△— —, $(\overline{w^2}/U_\infty^2)^{-\frac{1}{4}}$.

directions, in agreement with the well-known Phillips (1955) theory for potential flow fluctuations. The total turbulent energy exhibits an essentially constant value at the wake centre.

Full symbols are for intermittent turbulent fluid. It is interesting that the lateral fluctuations $\overline{v^2}$ tend to vary proportionately less across the wake. One explanation for this behaviour was offered by Bradshaw (1967).

7.5. *Potential fluctuations*

Phillips (1955) derived rigorously that outside a stationary two-dimensional turbulent flow region (where $\gamma = 0$) the intensity of each of three components of induced potential fluctuations decays as $\frac{1}{4}$ power with lateral distance. In the same paper it was independently derived that for the same flow $\overline{v^2} = \overline{w^2} + \overline{u^2}$. In recent years there were few experimental checks of the possible extension of Phillips theory into intermittent potential bulges in the region where the intermittency factor is different from zero. Kovasznay, Kibens & Blackwelder (1970), and Thomas (1973) have found that the '$\frac{1}{4}$ power law' does fit experimental data for $\overline{u_p^2}$ in intermittent regions of a turbulent boundary layer and the two-dimensional turbulent wake respectively.

Wygnanski & Fiedler (1970) found that all three components $\overline{u_p^2}$, $\overline{v_p^2}$ and $\overline{w_p^2}$ decay according to the '$\frac{1}{4}$ power law' in the intermittent part of the two-dimensional mixing region. They found also that the second part of the Phillips theory $\overline{v_p^2} = \overline{u_p^2} + \overline{w_p^2}$ was also satisfied on 'the conditional basis' in the intermittent region.

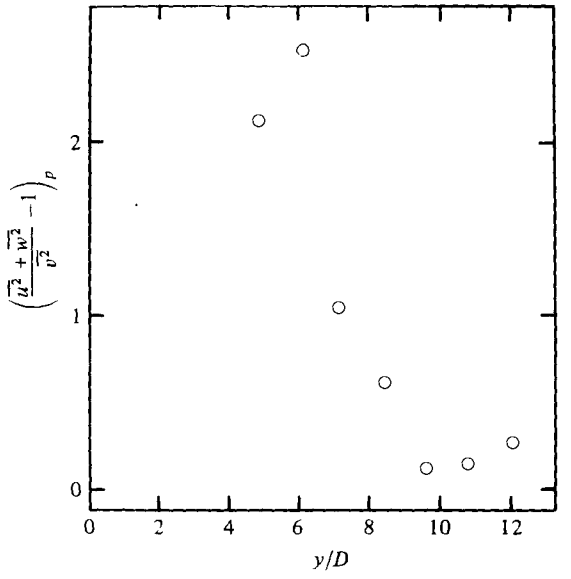

FIGURE 26. Check of sum of potential fluctuations in intermittent zones, R-averaged; $x/D = 400$.

Our results shown in figure 25 indicate reasonable agreement with the '$\frac{1}{4}$ power law'; however, if we check the other parts of the Phillips theory large disagreements were found close to the wake centre-line as is indicated in figure 26. Originally we were surprised by this result in the light of the good agreement found by Wygnanski & Fiedler (1970). We reviewed other available conditional sampling data for stationary two-dimensional turbulent flows, such as those on boundary layers by Kovasznay *et al.* (1970) and by Hedley & Keffer (1974) as well as available data on two-dimensional jet flow, and found that they all indicate substantial disagreement with the equality $\overline{v_p^2} = \overline{u_p^2} + \overline{w_p^2}$ in the intermittent region. Accordingly, it appears that the results found by Wygnanski & Fiedler (1970) in the mixing region represent an exception rather than the rule.

7.6. *The temperature fluctuations*

Figure 27 gives the temperature fluctuations profiles. The fluctuations computed with respect to the usual Reynolds averages achieve locally very high levels in both the turbulent and potential zones. The Z-averaging removes this 'singular' behaviour and it appears that in the potential (unheated) fluid the fluctuations are in fact truly negligible. In the turbulent (heated) fluid the fluctuations remain significant even at the very edge of the wake, possibly reaching an asymptote. The Z-averages should be interpreted in the light of the mean-temperature information of figure 20. The peak fluctuations appear to correspond approximately to the inflexion points of the respective mean profiles.

At the centre-plane the ratio θ'/Θ of the r.m.s. fluctuation to the local maximum of the mean temperature is 0·25, while Freymuth & Uberoi (1969) report 0·21. LaRue (1974) 0·28 and LaCoste (1972) 0·255. These differences are a measure of scatter between difficult, nominally similar experiments by careful investigators.

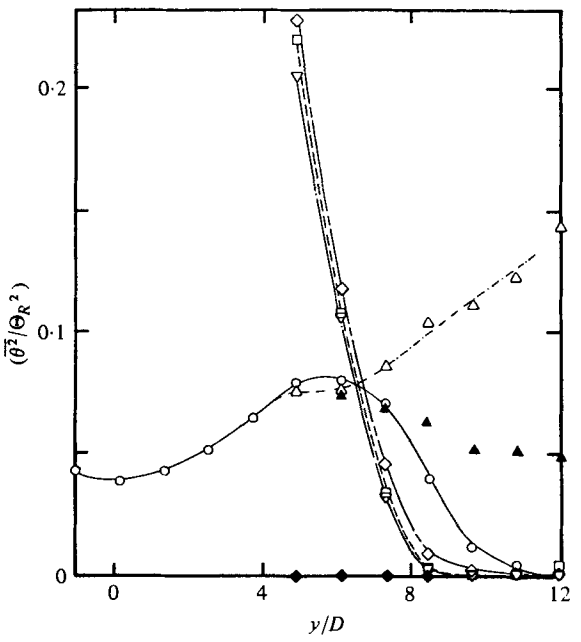

FIGURE 27. Conditional temperature fluctuations, $x/D = 400$. Symbols the same as on figure 18.

8. Second-order cross-correlations

Second-order cross-correlations are very important since they relate to the streamwise and lateral transport of momentum and heat. The most important off-diagonal component of the Reynolds stress tensor uv is, of course, also second-order cross-correlation.

8.1. *The $\overline{uv}$ correlation*

This correlation is often called the Reynolds shear stress since when multiplied by $-\rho$, the density, it performs the same role as the molecular stress $\mu\,\partial\overline{U}/\partial y$ in Reynolds's averaged equation for streamwise momentum. Figure 28 displays this correlation. Since the wake is symmetric, all $\overline{uv}$ correlations, no matter how averaged, are expected to be antisymmetric – hence the zero crossing in figure 28. Unlike $\overline{v^2}$ and $\overline{w^2}$, the $\overline{uv}$ stress component is 'fed directly' from the main stream through a 'production term' $\overline{v^2}\,\partial\overline{U}/\partial y$ (Hinze 1959, p. 251). It is therefore interesting that the maximum of the Reynolds stress does occur about where the product of $\overline{v^2}$ from figure 22, with the defect slope from figure 18, is largest. The turbulent bulges, i.e. the averages in the heated zones, have a significant level of Reynolds stress throughout. The cross-correlation $\overline{uv}$ is supposed to be zero in irrotational flow. However, the R-averaged Reynolds stress of the unheated potential zones increases substantially with proximity to the wake centre. The fronts of the turbulent bulges follow the same rising trend, while the backs are associated with an almost constant level of the Reynolds stress.

When the Reynolds stress is computed with respect to the local conditional averages, the values in the cold potential zones drop nearly to zero. The slight departure from zero is gratifying because it is confirmation that the various crucial

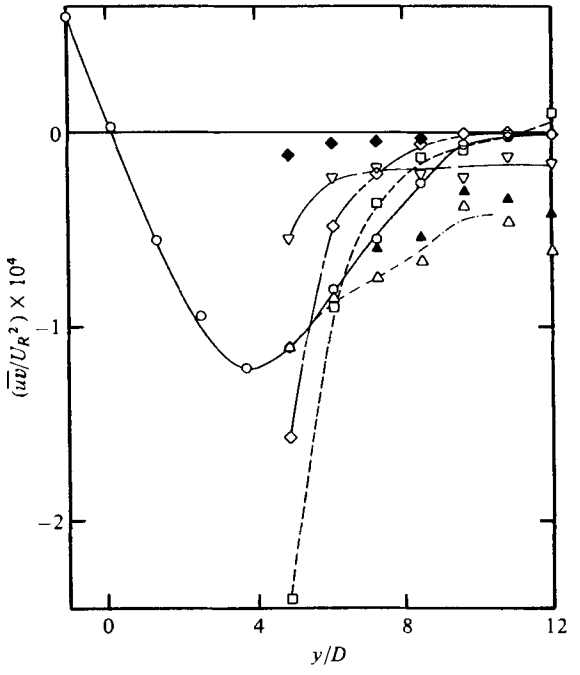

FIGURE 28. Reynolds stress, $x/D = 400$. Symbols the same as on figure 18.

practical compromises on the threshold criteria for potential zones, on the size of the probe, on hot-wire sensitivities for u and v measurements, on the sampling time, etc., had been made judiciously enough to yield significant results in quite delicate measurements. We should remark that the larger non-zero $\overline{uv}$ R-average values in the potential zones are not 'wrong'. They simply illustrate the consequences of Reynolds-type averaging with its single reference base. With respect to that base the cold irrotational lumps indeed contribute to the increase of exchange of the streamwise momentum per unit 'cold volume' at the rate $\partial(-\rho\overline{uv}_{R,\,\mathrm{cold}})/\partial y$.

In the turbulent zones the Z-averages of $\overline{uv}$ remain appreciable with a possible asymptote on the order of 25 per cent of the maximum. It is interesting that the rest of the Z-averages are essentially constant throughout the intermittent region.

Figure 29 gives the same correlations, but computed with the free-stream conditions as base. The conventional average shows the defect of the wake to move outwards from the wake centre. It is approximately proportional to the mean velocity gradient. The transfer by turbulent bulges remains high at the edges. The potential bulges transfer the defect toward the wake centre. The fronts and backs of the turbulent zones now correspond to momentum transfer of opposite sign. The latter is remarkably independent of lateral position.

8.2. *The $\overline{u\theta}$ correlation*

This correlation represents the minor portion of the heat flux (actually the multiplier $c_p\rho$ should be included) across fixed vertical planes (the major portion is heat convection $\overline{U\Theta}$) and appears in the slow-changing x-derivative in the equation for the mean temperature. It is therefore often neglected. However, since there is similarity

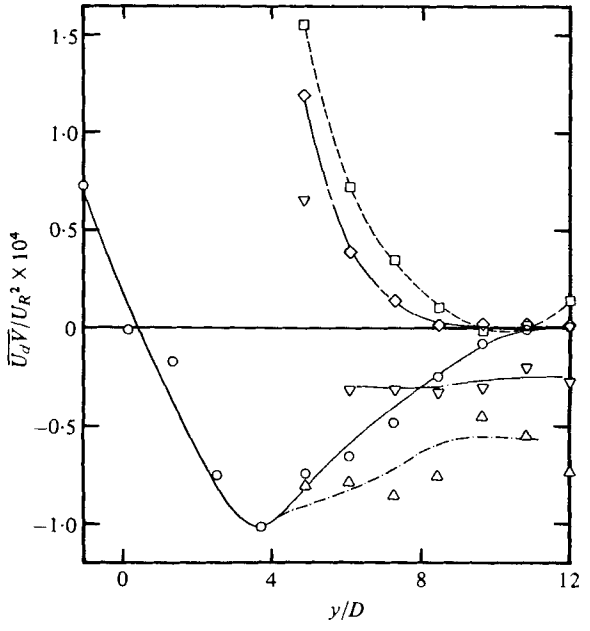

FIGURE 29. $\overline{U_d V}$ correlation; $x/D = 400$. Symbols the same as on figure 18.

in the lateral transfer of momentum defect and temperature, significant anti-correlation may be expected between these fluctuations. The knowledge of the $\overline{u\theta}$ variation thus should add to our appreciation of the physical processes.

Practically all experimental points in figure 30 show a negative correlation: the slower lumps are warmer. The conventionally averaged profile in figure 30 resembles a mirror image of a 'cross' between the $\overline{u^2}$ and $\overline{\theta^2}$ variations in figures 21 and 27. In particular the peak of $\overline{u\theta}$ occurs in between the peaks of $\overline{u^2}$ and $\overline{v^2}$. The variation of the Z-average in turbulent zones is not much lower than the R-average, while in the potential zones it is virtually zero.

Figure 31 shows the heat convection associated with the velocity defect. It represents only a few per cent of actual heat convected, but the streamwise heat transport due to fluctuations (figure 3) is, even for one order of magnitude, lower than that due to the velocity defect.

8.3. *The $\overline{v\theta}$ correlation*

This is a very important correlation since it characterized the lateral transport of heat per unit area of planes (y = constant). The lateral gradient of this correlation dominates the redistribution of the mean thermal energy laterally, and its product with the lateral gradient of temperature is responsible for the main production rate of temperature fluctuations $\overline{\theta^2}$. Figure 32 is computed with respect to the conventional averages. The warm turbulent fluid (the curve which coincides with the conventional average in the body of the wake) transfers increasingly more heat from the wake centre as y increases within the turbulent fluid. A considerable amount of heat is transferred by turbulent fluctuations within the intermittent turbulent bulges (Z-average). It is actually comparable to the heat transferred by outward-moving bulges themselves (product of conditional turbulent zone averages $\overline{V}$ and $\overline{\Theta}$).

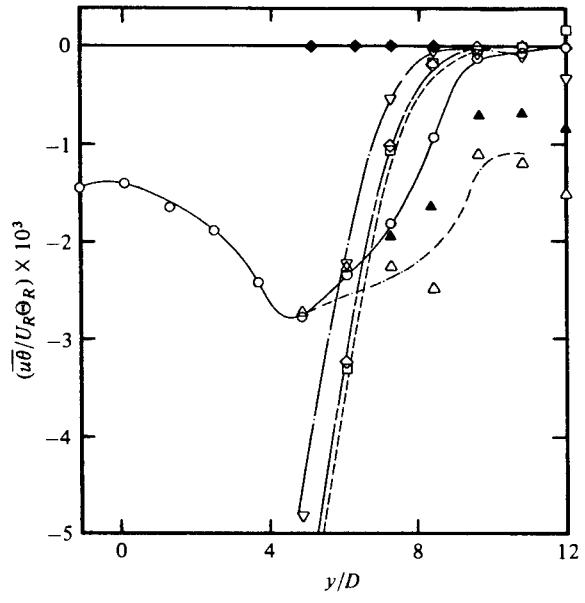

FIGURE 30. $\overline{u\theta}$ correlation; $x/D = 400$. Symbols the same as on figure 18.

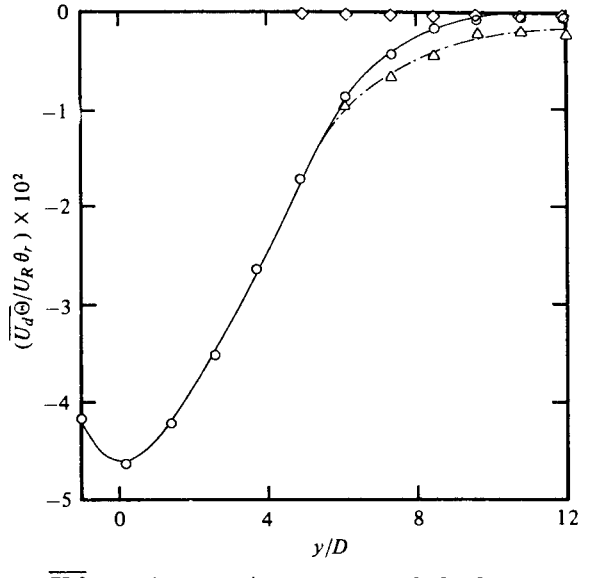

FIGURE 31. $\overline{U_d\theta}$ correlation, $x/D = 400$. Symbols the same as on figure 18.

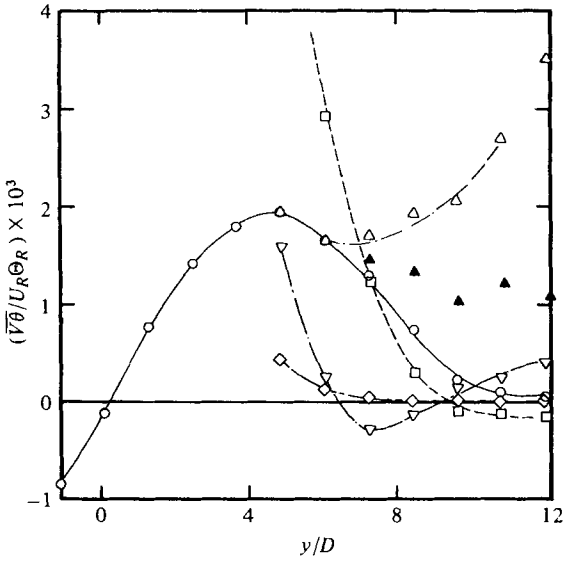

FIGURE 32. $\overline{v\theta}$ correlation, $x/D = 400$. Symbols the same as on figure 18.

Figure 33 displays the same correlations referenced to $\overline{\Theta}$ and $\overline{V}$ of zero (free-stream values) presenting the rate of lateral heat transfer. The rate in the turbulent fluid still increases constantly as the wake periphery is approached.

9. Second-order correlation coefficients

Dividing second-order correlations of two fluctuating quantities by r.m.s. values of the fluctuation quantities, one obtains correlation coefficients. They are non-dimensional indicators of the degree of organized association of the two instantaneous fluctuations.

Figure 34 displays the profile of the Reynolds stress correlation coefficient. The conventional profile resembles the profile of the Reynolds stress itself. However, this time the maximum is much broader, extending relatively higher values toward the wake edge. This is a measure of level of 'specific' momentum exchange by local turbulent fluctuations. The maximum level exceeds 0·5, which is about the same as that for the turbulent wake of a thin plate as measured by Kovasznay & Ali (1974), and close to the value obtained by Bradbury (1965) for the plane turbulent jet. In turbulent zones the correlation increases only slightly while the Reynolds stress increases rather steeply. The correlation reaches values near unity for short potential bulges close to the central region. When zone averages are used to compute the correlation coefficient almost no noticeable decrease can be observed in the turbulent zones; however, values in the potential zones are considerably lower.

Figure 35 displays the correlation coefficient of fluctuations of the streamwise velocity and temperature. This correlation coefficient has a maximum of over 0·6. The position of the maximum is substantially closer to the wake edge than in $\overline{uv}/u'v'$, with a relatively rapid drop-off at the edge. It is possible that this decrease in the correlation at the edge is due to the relative acceleration of the tops of the turbulent bulges by faster-moving potential flow, especially in the light of the fact that θ' was

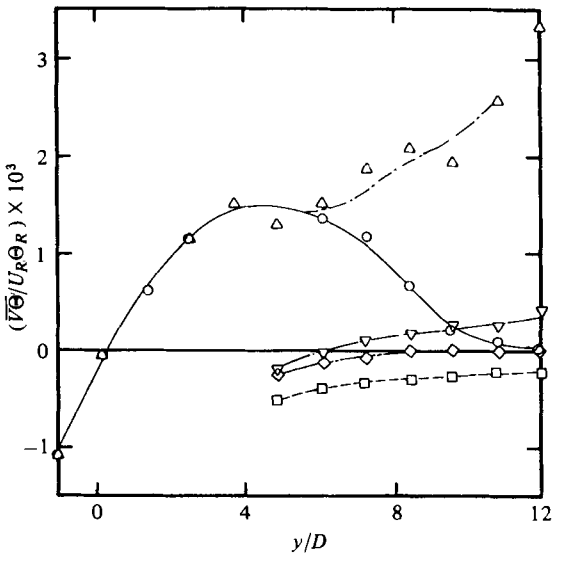

FIGURE 33. $\overline{V\Theta}$ correlation, $x/D = 400$. Symbols the same as on figure 18.

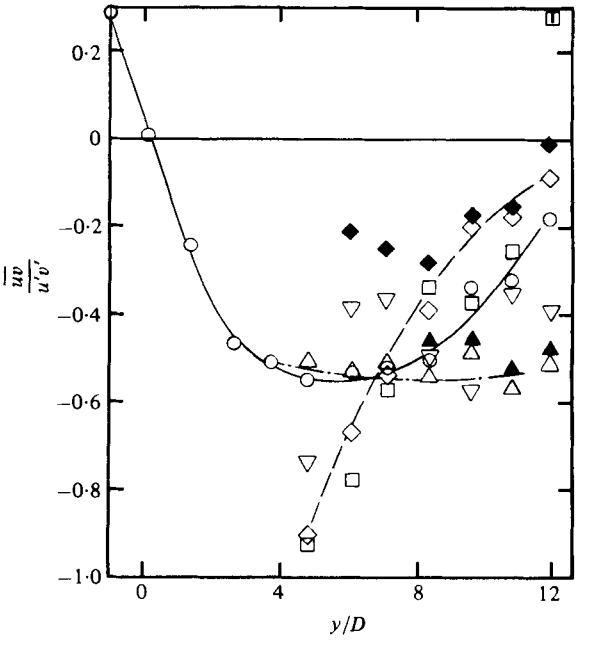

FIGURE 34. Correlation coefficient of u and v fluctuations, $x/D = 400$. Symbols the same as on figure 18.

about constant in this region. There were some indications of local displacement effect, so that some parts of the fluid were moving faster than the average potential flow, for example at the fronts of turbulent bulges. Zone averaging brings only slight decrease of the values in the turbulent zones. A plot was not made for the potential zones, since no temperature fluctuations are existent there. In the wake central region this correlation coefficient exhibits only a shallow minimum value of 0·48.

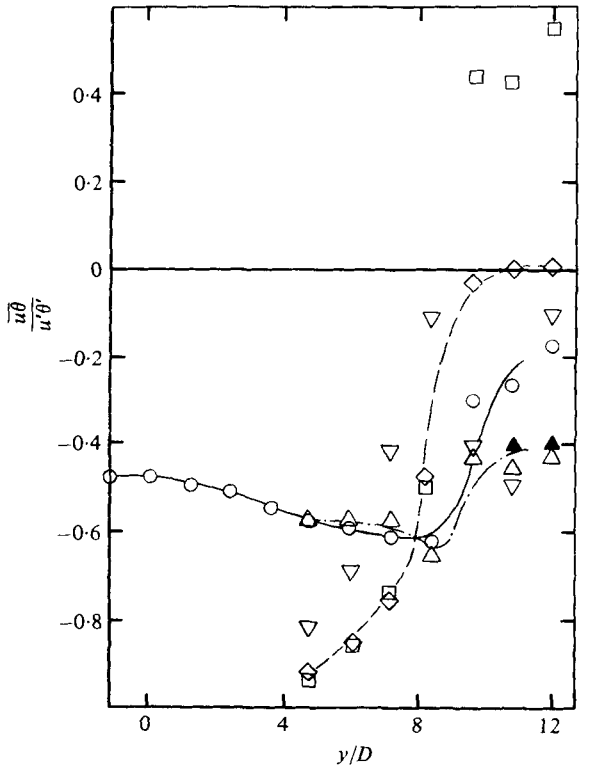

FIGURE 35. Correlation coefficient of u and θ fluctuations, $x/D = 400$. Symbols the same as on figure 18.

Figure 36 shows the correlation coefficient profiles for lateral velocity and temperature fluctuations. It is a measure of specific intensity of lateral heat transfer by these fluctuations. The conventional profile is similar to the correlation coefficient of uv fluctuation. The maximum value exceeds 0·5 and an almost constant value is maintained all the way up to the edge of the wake. Similar behaviour was observed in the wake of a plate by Kovasznay & Ali (1974). It is interesting that the correlation coefficient increases in turbulent zones exceeding a value of 0·7. The backs of the turbulent regions have values close to those of the potential zones near the wake centre and to those in turbulent zones at the wake edge. In between there is even a change of sign, meaning that relatively colder fluid is transported away from the wake centre. Similar correlation variations were obtained at the fronts of the turbulent zones.

When Z-averaged fluctuations are used the correlation coefficient maintains a constant value throughout the turbulent intermittent region.

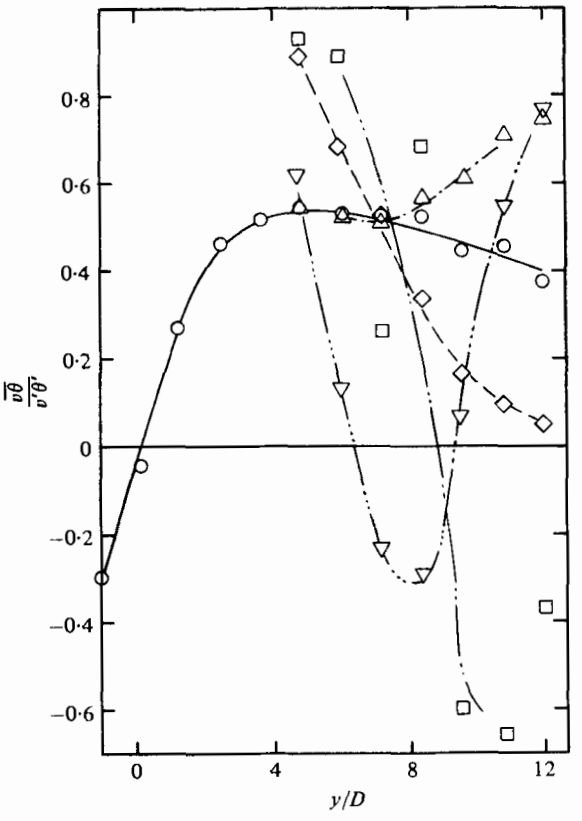

FIGURE 36. Correlation coefficient of v and θ fluctuations, $x/D = 400$. Symbols the same as on figure 18.

10. Principal stress axes

The orientation of one of the principal stress axes is illustrated in figure 37. The angle α_{s_1} is calculated from the expression

$$\alpha_{s_1} = \tfrac{1}{2}\tan^{-1}\left[\frac{2\overline{uv}}{\overline{u^2} - \overline{v^2}}\right].$$

The angle of the other principal axis is obtainable by adding or subtracting 90°.

In the region extending almost from the wake centre-line to two-thirds of its width α_{s_1} (for conventionally averaged velocities) is between $-30°$ and $-40°$ while at the periphery it is about $-65°$. Values for the potential and the turbulent zones as well as for the fronts and the backs do not deviate substantially from the conventional curve.

11. Summarizing remarks

Careful diagnostic studies were presented in the early sections of the paper. Their informative results showed that they were crucial in assuring reliability and repeatability of the wake data.

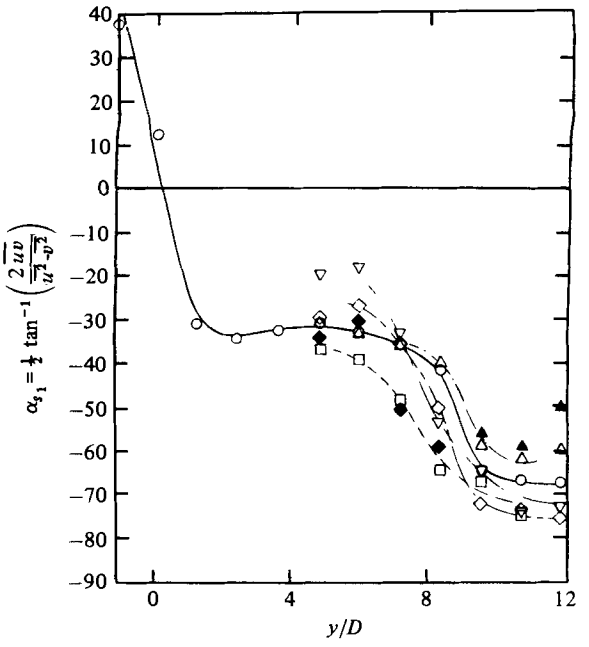

FIGURE 37. Angle of principal-stress axis with respect to X; $x/D = 400$. Symbols the same as on figure 18.

A number of improvements in signal processing were incorporated, increasing the accuracy of results. Some of the more important observations regarding the conditional wake data are as follows.

(1) Instantaneous traces of three components of velocity and temperature convincingly illustrate the fact that turbulent and potential zone flow characteristics are significantly larger than conventionally averaged mean flow properties. This means that if only mean flow is studied and predicted much of the important physical properties of turbulent flow would be lost. Accordingly, where possible, preference should be given to conditional sampling predictions in order to include the underlining physics.

(2) Instantaneous traces also seem to confirm the existence of 'deterministic' structures that are more or less quasi-periodic.

(3) Conditional velocity profiles indicate that the turbulent bulges are rolled over by faster-moving potential zones.

(4) Statistics of the length of turbulent zones agree reasonably with the properties of Gaussian distribution.

(5) Conventional u' and w' profiles agree reasonably with Townsend's measurements. Measured v' profiles, however, have significantly lower values in the central wake region and are slightly double peaked rather than single peaked. Crosscheck measurements and review of other data support our results.

(6) The measured value of $\theta'/\overline{\Theta} = 0{\cdot}255$ at the wake centre-line is in between the values of 0·21 obtained by Freymuth & Uberoi and of 0·28 obtained by LaRue, and is close to the value of 0·26 measured by LaCoste.

(7) Fluctuations computed with respect to zone averages have lower values than

when the conventional average is used as the reference. Decrease in the potential zones is more pronounced than in the turbulent zones. This is especially the case with the $\overline{uv}$ correlation that characterizes turbulent transport of momentum.

(8) It was found that the '$\frac{1}{4}$ power' law of decay of potential fluctuations outside a two-dimensional turbulent flow is satisfied even within the intermittent potential zones. However, the measurements indicate that the other (independently derived) part of the Phillips theory, $\overline{v_p^2} = \overline{u_p^2} + \overline{w_p^2}$, is not satisfied within the intermittent potential zones.

(9) Of all second-order correlation coefficients the lateral velocity temperature correlation has the highest values in the intermittent turbulent zones.

(10) Conventional correlation coefficients of u, v, θ reach maximum values of 0·5 to 0·6. The values of the R-averaged correlation coefficients approach unity in the potential zones close to the wake central region.

(11) The angle (α_s) of the principal stress axis in the main body of the wake is relatively close to $-45°$ which is the approximate orientation of the principal axis of the strain tensor since $\partial\overline{U}/\partial y$ is much higher than $\partial\overline{V}/\partial x$. However, at the wake periphery α_s is $-60°$ to $-70°$ indicating that $\partial\overline{V}/\partial x$ probably becomes comparable to $\partial\overline{U}/\partial y$.

Numerous discussions with Dr M. V. Morkovin and Dr J. L. Way and their encouragement during this research were invaluable.

This research was supported by USAF OSR Grant no. AFOSR-73–2509.

REFERENCES

Alexopoulos, C. C. & Keffer, J. F. 1968 *Rep.* 6811, *University of Toronto.*
Antonia, R. A., Prabhu, A. & Stephenson, S. E. 1975 *J. Fluid Mech.* **72**, 455.
Bevilaqua, P. M. & Lykoudis, P. S. 1971 *A.I.A.A. J.* **9**, 1657.
Blackwelder, R. F. & Kovasznay, L. S. G. 1972 *J. Fluid Mech.* **53**, 61.
Bradbury, L. J. S. 1965 *J. Fluid Mech.* **23**, 31.
Bradshaw, P. 1967 *J. Fluid Mech.* **30**, 241.
Corsin, S. 1943 *N.A.C.A.* WR–94.
Corsin, S. & Uberoi, 1950 *N.A.C.A. Rep.* 998.
Crow, L. E., Davis, F. A. & Maxfield, M. W. 1960 *Statistical Manual.* Dover.
Fabris, G. 1974 Doctoral Dissertation, Illinois Institute of Technology.
Fabris, G. 1978 *Rev. Sci. Instrum.* **49** (5), 654.
Freymuth, P. & Uberoi, M. S. 1969 *Phys. Fluids* **12**, 1359.
Freymuth, P. & Uberoi, M. S. 1971 *Phys. Fluids* **14**, 2574.
Goldschmidt, V. & Young, M. F. 1973 *Rep.* HL 73–31, *Purdue University.*
Grant, H. L. 1958 *J. Fluid Mech.* **4**, 149.
Hedley, T. B. & Keffer, J. F. 1974 *J. Fluid Mech.* **64**, 645.
Hinze, J. O. 1959 *Turbulence.* New York: McGraw-Hill.
Jenkins, P. E. 1975 Doctoral Dissertation, Purdue University.
Keffer, J. F. 1965 *J. Fluid Mech.* **22**, 135.
Keffer, J. F. 1967 *J. Fluid Mech.* **28**, 183.
Kotsovinos, N. E. 1975 Doctoral Dissertation, California Institute of Technology.
Kovasznay, L. S. G. 1948 *Proc. Roy. Soc.* A **198**, 174.
Kovasznay, L. G. S. & Ali, S. F. 1974 *Proc. 5th Int. Heat Trans. Conf., Tokio*, vol. 2, p. 99.
Kovasznay, L. S. G., Kibens, V. & Blackwelder, R. F. 1970 *J. Fluid Mech.* **41**, 283.

LaCoste, F. A. 1972 M.S. Dissertation, Pennsylvania State University.
LaRue, J. 1974 Doctoral Dissertation, University of California at San Diego.
LaRue, J. & Libby, P. A. 1974 *Phys. Fluids* **17**, 1956.
La Rue, J. & Libby, P. A. 1976 *Phys. Fluids* **19**, 1864.
Libby, P. A. 1976 *Phys. Fluids* **19**, 494.
Liepmann, H. W. & Laufer, J. 1947 *N.C.A.A. Tech. Note* 1257.
Lumley, J. L. & Panovsky, H. A. 1964 *The Structure of Atmospheric Turbulence.* New York: Interscience.
Papailiou, D. D. 1971 Doctoral Dissertation, Purdue University.
Phillips, O. 1955 *Proc. Camb. Phil. Soc.* **51**, 220.
Roshko, A. 1953 *N.A.C.A.* TN 2913.
Roshko, A. 1976 *A.I.A.A. J.* **14** (10), 1349.
Spencer, B. W. 1970 Doctoral Dissertation, University of Illinois.
Thomas, R. M. 1973 *J. Fluid Mech.* **57**, 549.
Townsend, A. A. 1947 *Proc. Roy. Soc.* A **190**, 551.
Townsend, A. A. 1948 *Aust. J. Sci. Res.* **1**, 161.
Townsend, A. A. 1949*a* *Proc. Roy. Soc.* A **197**, 124.
Townsend, A. A. 1949*b* *Aust. J. Sci. Res.* **2**, 451.
Wygnanski, I. & Fiedler, H. E. 1969 *J. Fluid Mech.* **38**, 577.
Wygnanski, I. & Fiedler, H. E. 1970 *J. Fluid Mech.* **41**, 237.